Skeletal Cut Loci on Convex Polyhedra*

Joseph O'Rourke Costin Vîlcu

June 25, 2025

Abstract

On a convex polyhedron P, the *cut locus* $\mathcal{C}(x)$ with respect to a point x is a tree of geodesic segments (shortest paths) on P that includes every vertex. We say that P has a *skeletal cut locus* if there is some $x \in P$ such that $\mathcal{C}(x) \subset \mathrm{Sk}(P)$, where $\mathrm{Sk}(P)$ is the 1-*skeleton* of P. At a first glance, there seems to be very little relation between the cut locus and the 1-skeleton, as the first one is an intrinsic geometry notion, and the second one specifies the combinatorics of P.

In this paper we study skeletal cut loci, obtaining four main results. First, given any combinatorial tree $\mathcal{T}$, there exists a convex polyhedron P and a point x in P with a cut locus that lies in $\mathrm{Sk}(P)$, and whose combinatorics match $\mathcal{T}$. Second, any (non-degenerate) polyhedron P has at most a finite number of points x for which $\mathcal{C}(x) \subset \mathrm{Sk}(P)$. Third, we show that almost all polyhedra have no skeletal cut locus. Fourth, we provide a combinatorial restriction to the existence of skeletal cut loci.

Because the source unfolding of P with respect to x is always a non-overlapping net for P, and because the boundary of the source unfolding is the (unfolded) cut locus, source unfoldings of polyhedra with skeletal cut loci are edge-unfoldings, and moreover "blooming," avoiding self-intersection during an unfolding process.

We also explore partially skeletal cut loci, leading to *partial edge-unfoldings*; i.e., unfoldings obtained by cutting along some polyhedron edges and cutting some non-edges.

1 Introduction

1.1 Background and Results

Our focus is the cut locus $\mathcal{C}(x)$ of a point x on a convex polyhedron P, and the relationship of $\mathcal{C}(x)$ to the 1-*skeleton* of P— the graph of vertices and edges— which we denote by $\mathrm{Sk}(P)$.

The *cut locus* $\mathcal{C}(x)$ of $x \in P$ is the closure of the set of points on P to which there is more than one geodesic segment (shortest path) from x. $\mathcal{C}(x)$ is a tree

*A preliminary version of this paper (excluding trees with degree-2 nodes and partially skeletal cut loci) was presented at a conference [OV24b].

whose leaves are vertices of P. Nodes of degree $k \geq 3$ are *ramification points* to which there are k distinct geodesic segments from x. Nodes v of degree 2 in $\mathcal{C}(x)$ can also occur, if v is a vertex of P. For details, see Section 1.2.

The 1-skeleton of a non-degenerate polyhedron is a 3-connected planar graph by Steinitz's theorem. We call a doubly-covered convex polygon a *degenerate* convex polyhedron, for which the 1-skeleton is a cycle.

We say that P has (or posesses) a *skeletal cut locus* if there is some $x \in P$ such that $\mathcal{C}(x) \subset \mathrm{Sk}(P)$. Such a polyhedron P is called *cut locus amenable*, *amenable* for short.

The edges of $\mathcal{C}(x)$ are known to be geodesic segments [AAOS97], so it is at least conceivable that an edge of $\mathcal{C}(x)$ lies along an edge of P. Theorem 1 shows that, for certain polyhedra P and points $x \in P$, all of $\mathcal{C}(x)$ lies in the 1-skeleton of P: $\mathcal{C}(x) \subset \mathrm{Sk}(P)$. As a simple example, we will see in Lemma 1 that the three edges incident to any vertex v_i of a tetrahedron form $\mathcal{C}(x)$ for an appropriate x, and are therefore a skeletal cut locus.

Although Theorems 2 and 3 will show that skeletal cut loci are "rare" in senses we'll make precise, Theorem 1 and its proof establish that uncountably many polyhedra do admit skeletal cut loci, in a sense made quantitatively precise by Proposition 1.

Theorem 4 characterizes those polyhedra every vertex of which has a skeletal cut locus. Complementing its first part, Theorem 5 provides a simple combinatorial restriction to the existence of skeletal cut loci, connecting to a current topic in graph theory.

Theorem 1 can also be viewed as a companion to the main result in [OV23], that any *length tree*—a tree with specified edge lengths—can be realized as the cut locus on some polyhedron. Here we only match the combinatorics of $\mathcal{T}$, not its metrical properties, but requiring additionally for $\mathcal{T}$ to be included in $\mathrm{Sk}(P)$.

Connection to Unfolding. It has long been known that cutting the cut locus $\mathcal{C}(x)$ and unfolding to the plane leads to the non-overlapping *source unfolding*: If x is not itself at a vertex, then the unfolding arrays all the shortest paths 2π around x, with the image of the cut locus forming the boundary of the unfolding [Mou85] [SS86]. For the polyhedra in Theorem 1, the source unfolding is an edge-unfolding. This adds another infinite class of polyhedra (which we call *tapered* in Section 11.4) that are known to have edge-unfolding *nets*. And because it is known that the source unfolding can be *bloomed*—unfolded continuously from $\mathbb{R}^3$ to $\mathbb{R}^2$ without self-intersection [DDH+11]—Theorem 1 and its companion Proposition 1 provide perhaps the first infinite class of examples of blooming edge-unfoldings.

A central open problem asks for an accounting of all the polyhedra P that support a skeletal cut locus. All of these enjoy the property that source unfoldings are also blooming edge-unfoldings.

In Section 8 we introduce and briefly explore partially skeletal cut loci, leading to *partial edge-unfoldings*; i.e., unfoldings obtained by cutting along some polyhedron edges and cutting some non-edges.

1.2 Cut Locus Preliminaries

For the readers convenience, we list next several basic properties of cut loci, sometimes used implicitly in the following.

(i) $\mathcal{C}(x)$ is a tree drawn on the surface of P. Its leaves are vertices of P, and all vertices of P, excepting x (if it is a vertex) are included in $\mathcal{C}(x)$. All points interior to $\mathcal{C}(x)$ of degree 3 or more are known as *ramification points* of $\mathcal{C}(x)$. All vertices of P interior to $\mathcal{C}(x)$ are also considered as ramification points, of degree at least 2; see e.g. Fig. 4.

(ii) Each point y in $\mathcal{C}(x)$ is joined to x by as many geodesic segments[1] as the number of connected components of $\mathcal{C}(x) \setminus y$. For ramification points in $\mathcal{C}(x)$, this is precisely their degree in the tree.

(iii) The edges of $\mathcal{C}(x)$ are geodesic segments on P.

(iv) Assume the distinct geodesic segments γ and γ' from x to $y \in C(x)$ bound a domain D of P, which intersects no other geodesic segment from x to y. Then there is an arc of $\mathcal{C}(x)$ at y which intersects D and bisects the angle of D at y.

(v) The tree $\mathcal{C}(x)$ is reduced to a path if and only if the polyhedron is a doubly-covered (planar) convex polygon, with x on the rim.

Further details and references can be found in [OV24a, Ch. 2].

2 Main Result and Examples

Our main result is the following theorem.

Theorem 1 *Given any combinatorial tree $\mathcal{T}$ there is a convex polyhedron P and a point $x \in P$ such that the cut locus $\mathcal{C}(x)$ is entirely contained in* $\mathrm{Sk}(P)$, *and the combinatorics of $\mathcal{C}(x)$ match $\mathcal{T}$.*

The proof of Theorem 1 is quite long. It consists of a case analysis (Section 11), a detailed construction for each (sub)case (Sections 9–10, 11.1, 11.2, 11.3, 11.4), and a concluding induction (Section 12). Rather than plunging right into the proof, we instead continue by sketching the main proof idea, and then presenting the consequences and implications of Theorem 1, postponing the proof details to Sections 9–12.

We next illustrate the main idea of the construction, with the simple case of a tree without degree-2 nodes. Suppose the given tree $\mathcal{T}$ is the 7-leaf tree shown in Fig. 1. We select a degree-3 node as root a, which corresponds to the apex of a regular tetrahedron $av_1v_2v_3$. We fix x at the centroid of the base Q.

Fig. 2(a) show one possible construction of P. The edges incident to a are clearly in $\mathcal{C}(x)$ with x at the centroid of the base triangle. All three base vertices

[1] We will sometimes abbreviate "geodesic segment" by *geoseg*, and "geodesic arc" by *geoarc*.

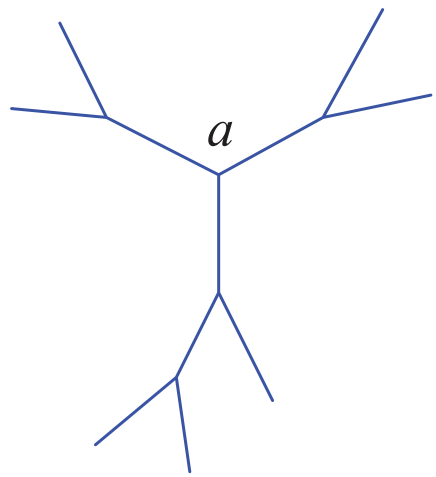

Figure 1: Tree $\mathcal{T}$ with 7 leaves.

of the tetrahedron are then truncated, with the truncation of v_1 truncated a second time. Now T corresponds to all the non-base edges of P.

The truncations are not arbitrary: the truncation planes must have precise tilts in order for the edges of each truncation to lie in $\mathcal{C}(x)$. Fig. 2(b) shows the source unfolding of P, with a_1, a_2, a_3 the three images of a. The red bisector rays from x through the truncation vertices on the base Q suggest that indeed any point p on a truncation edge is equidistant from x and therefore on $\mathcal{C}(x)$.

Returning to the need for precise tilts of the tuncation planes, let z be the point on the edge av_1 through which the truncation plane passes, creating a truncation triangle zt_1t_2. As indicated in Fig. 3, the tilt is uniquely determined by the location of z: the placement of z determines t_1, t_2, and the edge t_1t_2 determines z.

Vertex truncations naturally increase the degree of a polyhedron vertex, matching the degree of a node of $\mathcal{T}$. See, e.g., Fig. 12 in Section 10. One reason the proof of Theorem 1 is so long is that a degree-2 node of $\mathcal{T}$ cannot be created by the same basic truncation process. Instead we found it necessary to partition the possible occurrences of degree-2 nodes into four subcases (Fig. 14).

3 Theorem 1 Discussion

We mentioned in Section 1 that Theorem 1 leads to an uncountable number of skeletal polyhedra. This follows immediately from the freedom to place z at any point interior to av_1 in the construction detailed in Section 9. We can be more quantitatively precise, as follows.

Assume that $\mathcal{T}$ is a cubic tree without degree-2 nodes, so it has n leaves

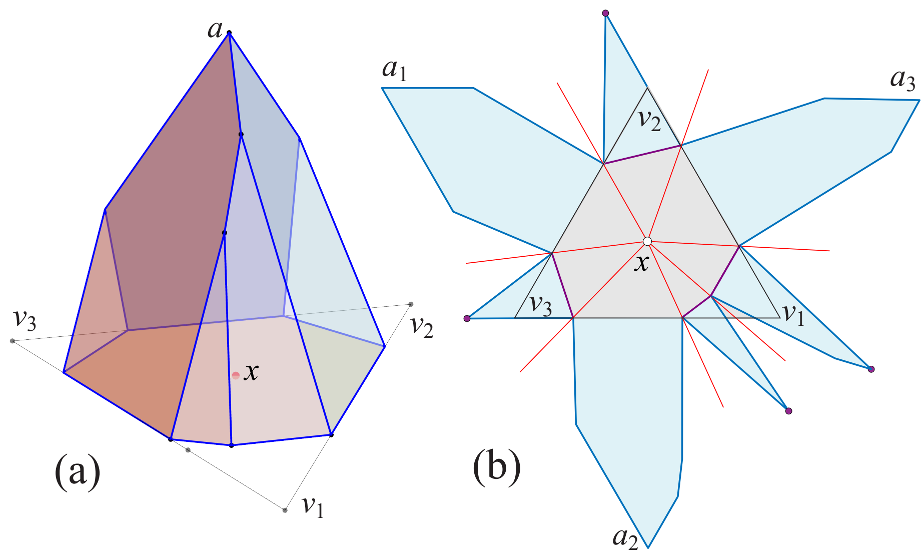

Figure 2: (a) P is created from a regular tetrahedron by four vertex truncations. $\mathcal{C}(x)$ consists of all non-base edges. (b) Source unfolding of P from x. Bisectors shown red.

and $n-2$ ramification points. Aside from one ramification point, which is chosen as the apex of the starting tetrahedron, all others are free to vary on their respective edges in our construction, which implies $n-3$ free parameters. Because $\mathcal{C}(x)$ is skeletal, each ramification point of $\mathcal{T}$ is a vertex of P, so P has $V = 2n-2$ vertices, and $n = V/2+1$. The space $\mathfrak{P}_V$ of all convex polyhedra with V vertices, up to isometries, has dimension $3V-6$ (see for example [LP22]), hence the starting tetrahedron provides another 6 free parameters and we have the next result.

Proposition 1 *The set of convex polyhedra admitting skeletal cut loci—and hence blooming edge-unfoldings—contains a subset of dimension $\geq V/2+4$ in the $(3V-6)$-dimensional space of all convex polyhedra with V vertices, up to isometries.*

Our construction for trees without degree-2 nodes in Theorem 1 (see Sections 2 and 9) results in a *dome*, a convex polyhedron P with a distinguished base face Q, with every other face sharing an edge with Q. It was already known that domes have edge-unfoldings [DO07, p. 325], although the proof of non-overlapping for our domes is almost trivial—the source unfolding does not overlap.

However, there are many other polyhedra with skeletal cut loci, see, e.g., Fig. 4, Theorem 4, Fig. 15, and Section 13. Which leaves us with this central open problem: *Characterize all convex polyhedra P which admit skeletal cut loci,*

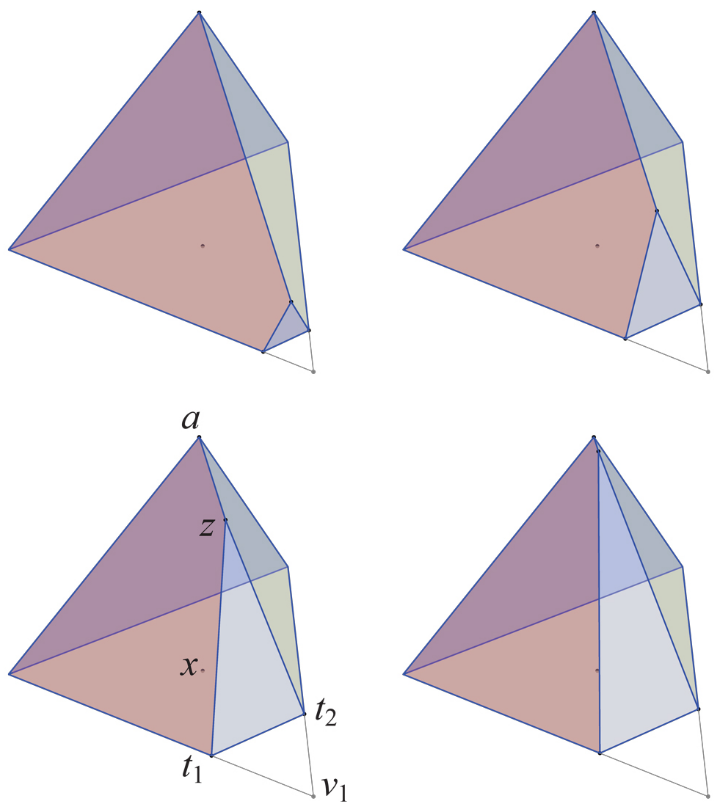

Figure 3: The tilt of the truncation plane is determined by the position of z on av_1.

i.e., characterize the *amenable* convex polyhedra. The remainder of the paper, before giving the main proof, addresses and partially answers this problem.

Several natural questions now suggest themselves:

(1) For a fixed P, how many distinct points x can lead to skeletal cut loci? (Theorem 2).

(2) Can all of $\mathrm{Sk}(P)$ for a given P be covered by several cut loci? (Proposition 2).

(3) How common / rare are skeletal cut loci in the space of all convex polyhedra? (Theorem 3).

(4) Are there restrictions for the existence of skeletal cut loci? (Proposition 2, Theorems 2 and 5).

4 Existence of Several Skeletal Cut Loci

In the first two questions in the list above, degenerate P play a special role:

Proposition 2 *(a) There exists infinitely many points x with $\mathcal{C}(x) \subset \mathrm{Sk}(P)$ if and only if P is degenerate.*

(b) There exists two points x_1, x_2 on P whose cut loci together cover $\mathrm{Sk}(P)$ if and only if P is degenerate.

The finitness claim in Theorem 2 is then a corollary of claim (a). Before arguing for a quantitative statement of this theorem, we make two observations. First, for P degenerate, $\mathrm{Sk}(P)$ is the rim of P, and for any x on the rim, $\mathcal{C}(x)$ is a subset of $\mathrm{Sk}(P)$. So one direction (a) of the proposition is trivial. Second, a special case asks whether it could be that each vertex v of P leads to a skeletal cut locus $\mathcal{C}(v)$. The answer is YES, realized, for example, by the regular octahedron.

Theorem 2 *For any non-degenerate P with E edges, there are at most $2\binom{E}{2}$ flat points x of P such that $\mathcal{C}(x) \subset \mathrm{Sk}(P)$.*

Proof: Assume there exists a flat point x of P, such that $\mathcal{C}(x) \subset \mathrm{Sk}(P)$. Then x belongs to one or two faces, $x \in F_j$, with $j \in \{1, 2\}$. Let F denote either F_1 if $j = 1$, or the union $F_1 \cup F_2$ if $j = 2$.

Denote by v_i, $i \geq 3$, the vertices of F, and by e_i the edge of $\mathcal{C}(x) \subset \mathrm{Sk}(P)$ incident to v_i and not included in F. Finally, denote by γ_i the geodesic segment from x to v_i.

Because $e_i \subset C(x)$, γ_i and e_i together bisect the complete angle at v_i, by the bisection property (iv) of the cut locus. In other words, the straight extensions E_i into F by all e_i are concurrent: they intersect at the point x.

Now we count all the possible locations x over all edges of P. Consider a pair of edges e_i, e_j. Each has possible edge extensions from each endpoint.

So the edge extensions are geodesic rays. Two such straight extensions could intersect several times on P. However, only their first intersection beyond the endpoints is a possible location for x. Each edge has two extensions, one from each endpoint, and because there are E straight extensions of the E edges of P, there are at most $2\binom{E}{2}$ possible locations for x. $\square$

So this theorem settles the other direction of Proposition 2(a).

Now we prove Proposition 2(b), that only degenerate P allows covering $\mathrm{Sk}(p)$ by only two cut loci.

Proof: If P is degenerate then any two points on its rim, but not on the same edge, satisfy the conclusion.

Assume now that P is non-degenerate and $x \in P$ such that $\mathcal{C}(x) \subset \mathrm{Sk}(P)$. Then $\mathcal{C}(x)$ has at least one ramification point of degree $d \geq 3$, as it is known that only degenerate P support path cut loci. The d edges of $\mathcal{C}(x)$ lie in at least 3 faces of P. Then there exists a cycle in $\mathrm{Sk}(P)$, formed by edges of those faces which are not in $\mathcal{C}(x)$. But such a cycle cannot be covered by only one other cut locus, which is a tree. $\square$

Example 1 *Consider a regular dipyramid P over a convex $2m+1$-gon; see Fig. 4. One can see that, for every midpoint x of a "base edge" e, $\mathcal{C}(x)$ is included in $\mathrm{Sk}(P)$. More precisely, $\mathcal{C}(x)$ contains all base edges other than e, and the two "lateral edges" opposite to x. In particular, this provides $2m+1$ such points, for $V = 2m+3$ vertices.*

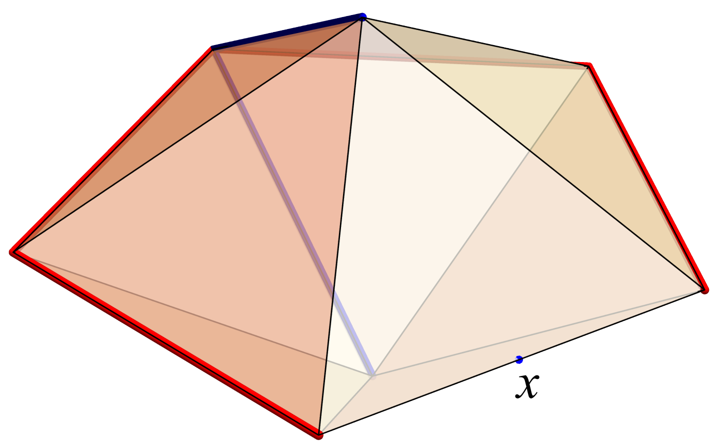

Figure 4: P: pentagonal dipyramid. $\mathcal{C}(x)$: red and blue edges of $\mathrm{Sk}(P)$.

5 Absence of Skeletal Cut Loci

The following lemma will explain a condition in Theorem 3 to follow.

Lemma 1 *Every tetrahedron T has four points $x \in T$ such that $\mathcal{C}(x) \subset \mathrm{Sk}(T)$.*

Proof: For each vertex v_i, denote by x_i the ramification point of $\mathcal{C}(v_i)$. It follows, from cut locus property (ii), that that v_i is the ramification point of $\mathcal{C}(x_i)$. Then, by (i) and (iii), $\mathcal{C}(x_i)$ consists of the three edges incident to v_i. $\square$

The next theorem establishes the rarity of skeletal cut loci. In the statement, by *almost all* we mean "all in an open and dense set" in $\mathfrak{P}_V$.

Theorem 3 *For almost all convex polyhedra P with $V > 4$ vertices, there exists no point $x \in P$ with $\mathcal{C}(x) \subset \mathrm{Sk}(P)$.*

Note that Lemma 1 establishes the need for $V > 4$.

Proof: Notice first that almost all convex polyhedra P are non-degenerate.

Assume, for the simplicity of the exposition, that every face of P is a triangle and $\mathrm{Sk}(P)$ is a cubic graph.

Case 1. Assume there exists a flat point x interior to some face F of P, such that $\mathcal{C}(x) \subset \mathrm{Sk}(P)$.

Repeating the notation in Theorem 2, denote by v_i, $i = 1, 2, 3$, the vertices of F, and by e_i the edges of P incident to v_i and not included in F. Moreover, denote by γ_i the geodesic segment from x to v_i.

As in Theorem 2, it follows that $e_i \subset C(x)$ so, together, γ_i and e_i bisect the complete angle at v_i. In other words, the straight extensions E_i into F by all the e_i are concurrent: they all intersect at the same point.

Now we perturb the vertices of P to destroy this concurrence. If P were a tetrahedron, then perturbing the apex would simultaneously move the edges incident to it. But the assumption that $V > 4$ means that there are at least two vertices outside the 3-vertex face F containing x. Perturbing these two vertices independently moves the edges incident to F independently, breaking the concurrence at x.

Because there are at most finitely many such points x by Theorem 2, the conclusion follows in this case.

Case 2. Assume there exists a flat point x interior to some edge e of P, such that $\mathcal{C}(x) \subset \mathrm{Sk}(P)$. Denote by v_i, $i = 1, 2$, the vertices of e, and by e_i the edges of P incident to v_i included in $\mathcal{C}(x)$. As above, it follows that the straight extensions of e_1, e_2 coincide with e. Now, small perturbations of the vertices of P destroy this coincidence. Note that if e, e_1, e_2 form a triangle, then e_1, e_2 will move together. But still, perturbations at other vertices of P (not $v_1, v_2, e_1 \cap e_2$) will destroy the concurrence.

Case 3. Assume finally there exists a vertex v of P, such that $\mathcal{C}(v) \subset \mathrm{Sk}(P)$. Here we obtain again that the straight extensions of two edges contain (other) edge-pair extensions, and small perturbations of the vertices of P destroy this coincidence.

□

We mentioned the simple fact that, for the regular octahedron, for every vertex v, $\mathcal{C}(v)$ is skeletal. In the next section we detail the special conditions such polyhedra must satisfy.

6 Every Vertex a Skeletal Source

By Theorem 3, few convex polyhedra P have a point x with $\mathcal{C}(x) \subset \mathrm{Sk}(P)$. So assuming that every vertex of P has this property should yield some exceptional polyhedra.

Theorem 4 *Assume that every vertex of P has a skeletal cut locus. Then the following statements hold.*

1. *Every face of P is a triangle.*
2. *Every vertex of P has even degree in* $\mathrm{Sk}(P)$.
3. *The edges at every vertex v split the complete angle at v into evenly many sub-angles, every two opposite such angles being congruent.*
4. *If, moreover, every vertex of P has degree 4 in* $\mathrm{Sk}(P)$ *then P is an octahedron:*
    - *with three planar symmetries, and*
    - *all faces of which are acute congruent (but not necessarily equilateral) triangles.*

Proof:

(1) Assume there exists a non-triangular face F of P, so there are non-adjacent vertices u, v of F. Because $v \in C(u) \subset \mathrm{Sk}(P)$, there exists an edge vw of P with $vw \subset C(u)$. Moreover, the diagonal uv of F and vw bisect the complete angle at v.

Because vw is an edge, it is a geodesic segment from w to v. So v is a leaf of $\mathcal{C}(w)$, and $\mathcal{C}(w)$ starts at v in the direction of the diagonal vu, hence $\mathcal{C}(w) \not\subset \mathrm{Sk}(P)$.

(2) Consider now a vertex u of P of degree d in $\mathrm{Sk}(P)$, and denote by $u_1, \ldots, u_d$ its neighbors in $\mathrm{Sk}(P)$.

For every u_i, $i = 1, \ldots, d$, u is a leaf of $\mathcal{C}(u_i)$, so the edge $u_i u$ and the edge of $\mathcal{C}(u_i) \cap \mathrm{Sk}(P)$ at u bisect the complete angle at u. Hence the edges at u can be paired two-by-two, hence their number is even.

(3) Denote by $e_1, \ldots, e_k, e_{k+1}, \ldots, e_{2k}$ the edges sharing the vertex u, indexed circularly, and put $\alpha_i = \angle(e_i, e_{i+1})$, with index equality $2k + 1 = 1$.

The bisecting property of cut loci implies that the edge e_1 (as a geodesic segment from vertex u_1 to u) and the edge e_{k+1} (as the branch of $\mathcal{C}(u_1)$ at leaf u) bisect the complete angle at u:

$$\sum_{i=1}^{k} \alpha_i = \sum_{i=1}^{k} \alpha_{k+i}.$$

Similarly,

$$\sum_{i=2}^{k+1} \alpha_i = \sum_{i=2}^{k+1} \alpha_{k+i}.$$

Subtracting, we get $\alpha_1 = \alpha_{k+1}$.

Analogous reasoning implies the other equalities: $\alpha_i = \alpha_{k+i}$, with index equality $2k + j = j$.

(4) For the combinatorial part, denote by F, E, V the number of faces, edges, and respectively vertices of P. Euler's formula for convex polyhedra gives $F - E + V = 2$. Our assumptions imply $3F = 2E$, and $4V = 2E$. These equations yield $V = 6$ and $F = 8$, hence P is an octahedron.

Denote by u, v, a, b, c, d the vertices of P, with a, b, c, d neighbor to both u and v.

Applying the hypothesis for a, b, c, d shows that the cycle $C = abcda$ in $\mathrm{Sk}(P)$ is a bisecting polygon. Therefore, there exists a local isometry ι of the 'upper' and 'lower' neighborhoods N_u, N_v of C. In particular, the curvatures at u and v are equal, by Gauss-Bonnet.

It follows even more, that the local isometry ι extends to an intrinsic isometry between the 'upper' and the 'lower' closed half-surfaces bounded by C (regarding them as cones), hence it further extends to an isometry of P fixing C. Therefore, C is planar and P is symetric with respect to the respective plane, by the rigidity part of Alexandrov's Gluing Theorem.

Repeating the reasoning for other pairs of 'opposite' vertices shows that all faces of P are congruent triangles.

The four faces sharing the vertex u have congruent angles at u, hence those angles are acute.

$\square$

Example 2 *Suitable dipyramids over convex $2m$-gons, similar to Example 1, provide non-octahedron polyhedra whose the cut loci of the vertices cover the 1-skeleton.*

7 A Combinatorial Restriction

Already mentioned in the Abstract, at a first glance there seems to be very little relation between the cut locus and the 1-skeleton, as the first one is an intrinsic geometry notion, and the second one specifies the combinatorics of P. A background connection between the two notions can however be established in two steps: Alexandrov's Gluing Theorem connects the intrinsic and the extrinsic geometry of P, while Steinitz's Theorem relates the combinatorics to the extrinsic geometry.

In this section we provide an easy combinatorial restriction to the existence of skeletal cut loci for cubic graphs, complementing the first part of Theorem 4.

In the literature, a spanning tree without degree-2 nodes is called a *HIST*.[2] So every spanning tree of a HIST-free graph has a degree-2 node.

Theorem 5 *A HIST-free cubic polyhedral graph cannot be realized with skeletal cut loci.*

Proof: Lemma 2.8 in [OV24a] shows that, at a vertex v of P of degree 3 in $\mathrm{Sk}(P)$, the sum of any two face angles is strictly larger than the third angle. Therefore such a degree-3 v in the graph cannot be a degree-2 node in a cut locus, because of Property (iv) of cut loci. $\square$

Open Problem 1 *Theorem 5 provides a necessary condition for a cubic polyhedral graph to be realizable with a skeletal cut locus. Is it also sufficient?*

Corollary 1 *Among the Platonic solids, only the regular tetrahedron and the regular octahedron have skeletal cut loci.*

Proof: Notice first that all tetrahedra have skeletal cut loci (Lemma 1), as does the regular octahedron, because it is a special case of Theorem 4 and Example 2).

One can check straightforwardly that the cube and the dodecahedron graphs are HIST-free, hence these polyhedra do not admit skeletal cut loci by Theorem 5.

We clarify next the situation of the icosahedron I. By the proof of Theorem 2, the only candidate source points x are the centers of the faces. Direct considerations show that such a cut locus is not completely included in $\mathrm{Sk}(I)$, see Fig. 5. $\square$

The cube example shows there exist convex polyhedra admitting edge-unfoldings, but not skeletal cut loci.

[2] HIST abbreviates "homeomorphically irreducible spanning tree." See, e.g., [GNRZ24] and the references therein.

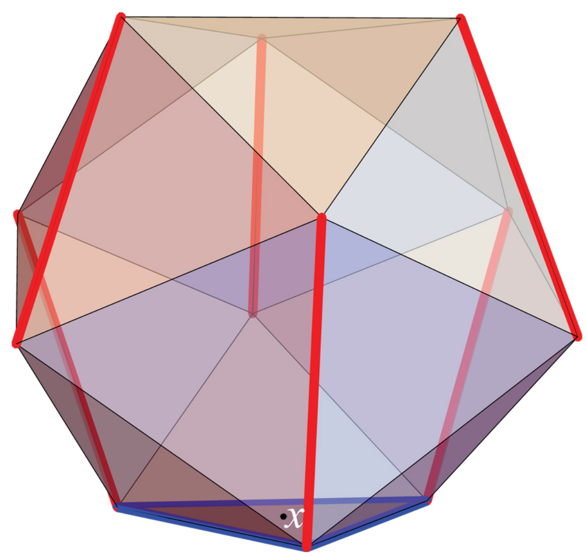

Figure 5: Source x is the center of the base face (blue). The six disjoint red edges are included in $\mathcal{C}(x)$, but none of the other polyhedron edges are in $\mathcal{C}(x)$. Therefore, $\mathcal{C}(x)$ must also include some non-edge geosegs to connect $\mathcal{C}(x)$ to a tree.

8 Partially Skeletal Cut Loci

Theorem 3 states that almost all convex polyhedra P with $V > 4$ vertices have no skeletal cut loci. This section is an attempt to roughly clarify "how far" are those polyhedra from having such cut loci.

Remark 1 *For every convex polyhedron P and each edge e of P, there are infinitely many points $x \in P$ such that $e \subset \mathcal{C}(x)$.*

Proof: Consider an extremity v of e, and the geodesic segment γ_v starting at v which, with e, bisects the complete angle at v. Also consider points x on γ_v sufficiently close to v. Then, either the proof of Theorem 2, or Property (iv) of cut loci in Section 1.2 on which it is based, directly implies $e \subset \mathcal{C}(x)$. $\square$

Fig. 5 indicates a point x on an icosahedron with 6 polyhedron edges in $\mathcal{C}(x)$, but several edges of $\mathcal{C}(x)$ are not part of the 1-skeleton.

Fig. 6 presents a cut locus which fails to be skeletal by a single edge. In our example the respective edge is internal, but minor changes show that it could as well be external. (An arc of a tree is called *external* it it is incident to a leaf, and *internal* otherwise.) We believe that Theorem 3 can be adapted to cover this case as well.

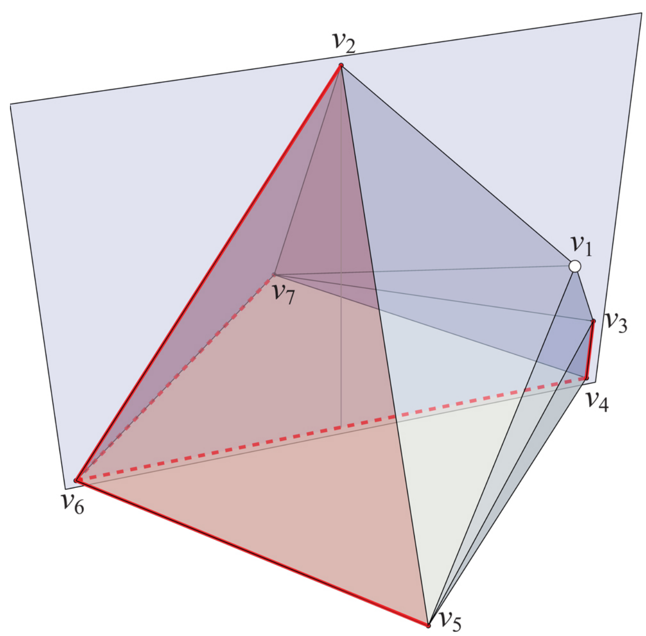

Figure 6: A convex polyhedron of 7 vertices and a vertical symmetry plane, obtained from a regular pyramid $v_2v_4v_5v_6v_7$. The cut locus $\mathcal{C}(v_1)$, drawn red, has 4 polyhedral edges and one non-polyhedral edge, v_4v_6.

For a non-degenerate convex polyhedron P, define $L(P) \geq 1$ as the maximal integer such that P admits a point x with $L(P)$ polyhedral edges in $\mathcal{C}(x)$. The quantity $L(P)$ can be regarded as a measure of how close is P to having skeletal a cut loci.

Direct considerations show that $L(C) = 4$ for the cube C, while $L(I) = 6$ for the icosahedron I (see again Fig. 5).

The proof of Theorem 1 can be easily adapted to provide examples of convex polyhedra and cut loci missing an arbitrary number of their edges[3] from being skeletal.

A *k-edge-unfolding* is an unfolding whose cut tree contains precisely k edges.

A *partial edge-unfolding* is an unfolding whose cut tree contains at least one edge, but it is not skeletal; so it is a k-edge-unfolding, for some $k \geq 1$. These unfoldings are obtained by cutting partially along edges and partially outside edges, so the concept is a bridge between edge-unfoldings (whose cut trees are composed by edges), and anycut-unfoldings (whose cut trees may contain no edge).

Remark 1 shows that every convex polyhedron admits a 1-edge-unfolding.

The following two questions are now natural, and related to Dürer's problem [O'R13]—whether or not every convex polyhedron has an edge-unfolding to a net.

Open Problem 2 *Find the maximal number $L_V \geq 1$ such that each non-degenerate convex polyhedron with $V \geq 5$ vertices*[4] *has a point whose cut locus contains L_V edges.*

In particular, does every convex polyhedron have a point with two edges in its cut locus?

Open Problem 3 *Find the maximal number $K_V \geq 1$ such that each non-degenerate convex polyhedron with V vertices has a $K(V)$ edge-unfolding to a net.*

Clearly $1 \leq L_V \leq K_V$, and Theorem 3 shows that, for $V > 4$, L_V cannot equal the number of edges of a spanning tree with $n = V/2 + 1$ leaves (see also the second paragraph in Section 3).

The part of the paper presenting comments on, and consequences of, Theorem 1 ends here. The remaining is devoted to the proof of Theorem 1, which consists of a case analysis (Section 11), a detailed construction for each (sub)case (Sections 9–10, 11.1, 11.2, 11.3, 11.4), and a concluding induction (Section 12).

[3] However, it doesn't work as such if one asks for the precise position of the non-polyhedral edges in the given tree.

[4] Notice that $L_4 = 3$, by Lemma 1.

9 Proof of Theorem 1, Case of no Degree-2 Nodes

Throughout this section we assume $\mathcal{T}$ has no degree-2 nodes. Start with P a pyramid with apex a centered over a regular n-gon base Q, with x the centroid of Q. Label the vertices of Q as $v_1, \ldots, v_n$.

The construction does not depend on the degree of apex a, so it is no loss of generality to assume a has degree-3 so that P starts as a regular tetrahedron. Let z be a node of $\mathcal{T}$ adjacent to a. (We will often use a and z and other variables to both refer to a node of $\mathcal{T}$ and a corresponding vertex of P.) Let z have degree $k+2$ in $\mathcal{T}$. Truncation of k planes through z will create a vertex at z of degree $k+2$. E.g., if z is degree-3, $k=1$ plane through z creates a vertex of degree-3, as we've seen in Fig. 3.

We aim to understand how to truncate $k \geq 1$ planes through z so that the $k+1$ truncation edges incident to the base Q are part of $\mathcal{C}(x)$. We will illustrate in detail the case $k=2$ shown in Fig. 7. Looking ahead, if we know how to construct k planes through z, then we can apply the same logic to construct j planes through a child y of z. The $j=1$ case is illustrated in Fig. 8, with the red truncation triangle incident to y. Then the same construction technique can be used to inductively create the full subtree rooted at z. We will show later that the subtrees rooted at the other two children of a can be arranged to avoid interfering with one another.

We express the construction as a multi-step algorithm, and later prove that the truncation edges are in $\mathcal{C}(x)$. Fix $k \geq 1$, and position z anywhere in the interior of av_1. The goal is to compute the *truncation chain* $t_1, t_2, \ldots, t_k, t_{k+1}$ on base Q, where $t_1 \in v_1v_n$ and $t_{k+1} \in v_1v_2$ (e.g., t_1, t_2, t_3 in Fig. 7). Each truncation triangle is then zt_it_{i+1}.

The construction of the truncation chain is effected by first computingd the unfolded positions z_i, the images of z in the unfolding. It is perhaps counterintuitive, but we can calculate z_i without knowing t_it_{i+1}; instead we use z_i to calculate t_it_{i+1}. The next construction depends of our choice of several parameters; we'll see later that it provides a suitable polyhedron.

(1) z_0 is the position of z unfolded with the left face of the tetrahedron, av_3v_1. z_0 can be determined by $|v_1z| = |v_1z_0|$. Then z_{k+1} is the reflection of z_0 across xv_1.

(2) Set $r_z = |xz_0| = |xz_{k+1}|$.

(3) All the z_i's are chosen to lie on the circle C_z centered on x of radius r_z.

(4) Let A be the angle z_0xz_{k+1}. Partition A into $k+1$ angles α. This is another choice, to maximize the symmetry of the construction.

(5) The z_i's lie on rays from x separated by α. Together with C_z, this determines the location of the z_i's.

(6) Set B_i to bisect the angle at x between the z_{i-1}, z_i rays, $i = 1, \ldots, k+1$.

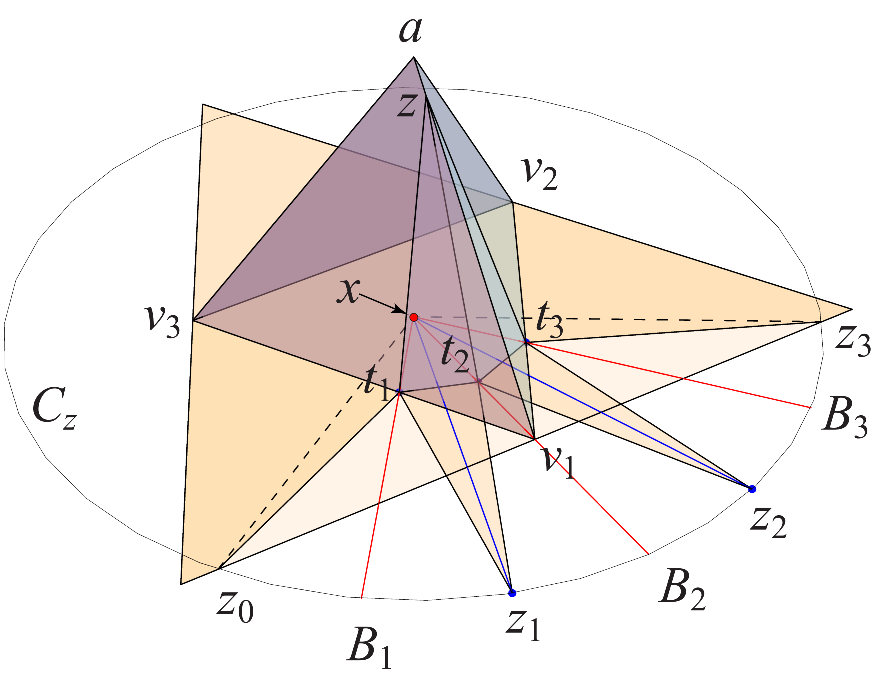

Figure 7: $k = 2$ truncation planes through z.

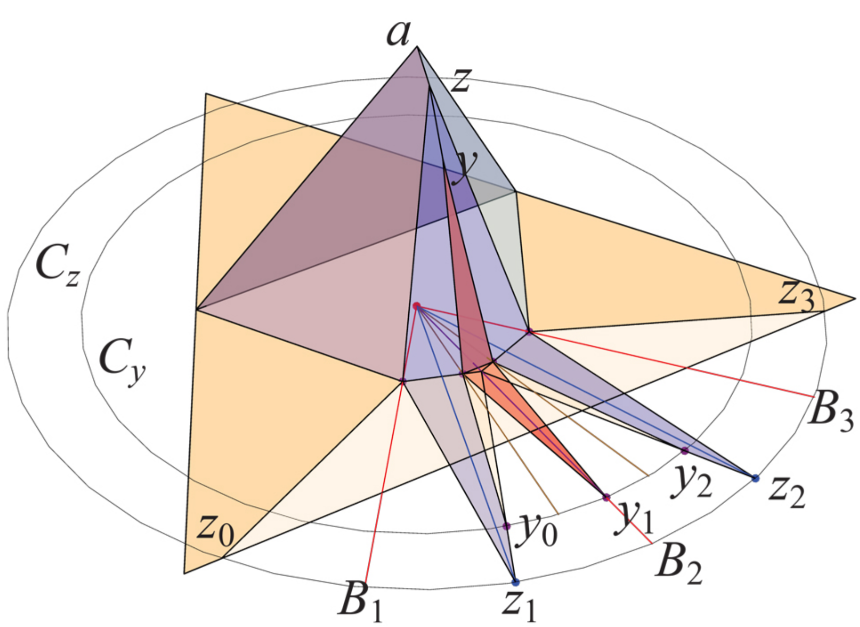

Figure 8: $k = 2$, $j = 1$. The y-truncation cuts the zt_2 edge in Fig. 7.

(7) We determine t_1 and t_{k+1} using the first and last bisector: $t_1 = v_1v_n \cap B_1$, $t_{k+1} = v_1v_2 \cap B_{k+1}$. The intermediate chain vertices $t_2, \ldots, t_k$ are not yet determined.

(8) Let Π_i be the mediator plane through zz_i, the plane orthogonal to zz_i through its midpoint. It is these planes that determine t_i, $i = 2, \ldots, k$.

(9) Π_i intersects the xy-plane in a line L_i containing t_it_{i+1}.

(10) $t_i = L_i \cap B_i$.

First note that the mediator plane construction of t_it_{i+1} guarantees that z unfolds to z_i. Second, the angles between edges t_iz_{i-1} and t_iz_i are split by B_i by construction. So any point p on the interior of edge zt_i unfolds to two images in the plane equidistant from x.

Lemma 2 *Each truncation edge zt_i is an edge of $\mathcal{C}(x)$.*

Proof: We first prove that zt_1 lies in $\mathcal{C}(x)$. Throughout refer to Fig. 9.

Before truncation, the segment zt_1 lies on the face av_3v_1 of the polyhedron P, which is a regular tetrahedron in this case.

Fix a point $p \in zt_1$. The unique shortest path γ to p crosses edge v_1v_3. After truncation, γ remains a geodesic arc. We aim to prove that it remains shortest, and moreover there is another companion geodesic segment γ', establishing that $p \in \mathcal{C}(x)$.

Now we consider the situation after truncation. Let δ be a geodesic arc from x to p, approaching p from the other side of zt_1; see Fig. 9(b). If δ crosses the edge t_1t_2, then we have $|\gamma| = |\delta|$ by construction, and we have found $\gamma' = \delta$.

Suppose instead that δ crosses edge t_it_{i+1} for $i \geq 2$, and then crosses the truncation triangles $zt_it_{i+1}, zt_{i-1}t_i, \ldots, zt_1t_2$ (right to left, i.e., clockwise, in Fig. 9(a)) before reaching p. To simplify the discussion, we illustrate $i = 2$, so δ crosses t_2t_3 and then triangles zt_2t_3 and zt_1t_2. See Fig. 9(b).

Let q_2 be the quasigeodesic[5] xt_2z on P'; it must be crossed by δ to reach p. There are two triangles xt_2z_1 and xt_2z_2 bounding q_2 to either side, congruent by the construction. Thus the construction has local intrinsic symmetry about q_2.

Let s be the point at which δ crosses t_2t_3, $\{s\} = \delta \cap t_2t_3$. First assume that s lies in the triangle xt_2z_2. Then δ remains in xt_2z_2 until it crosses q_2. Then there must be another geodesic arc δ' symmetric with δ about q_2, as illustrated in (b). So δ and δ' meet at a point of q_2. Because δ and δ' have the same length, neither can be a shortest path beyond that point of intersection. Therefore δ cannot reach p as a geodesic segment.

Second, if s instead lies in the triangle xt_3z_2, then it is clear from the planar image in (a) of the figure that δ cannot cross the segment xz_2 clockwise, which it must to reach p from the right in the figures. So δ must head counterclockwise, crossing $q_3 = xt_3z$. Then the same argument applies, based this time on the

[5]A *quasigeodesic* is a path with at most π surface to either side of every point.

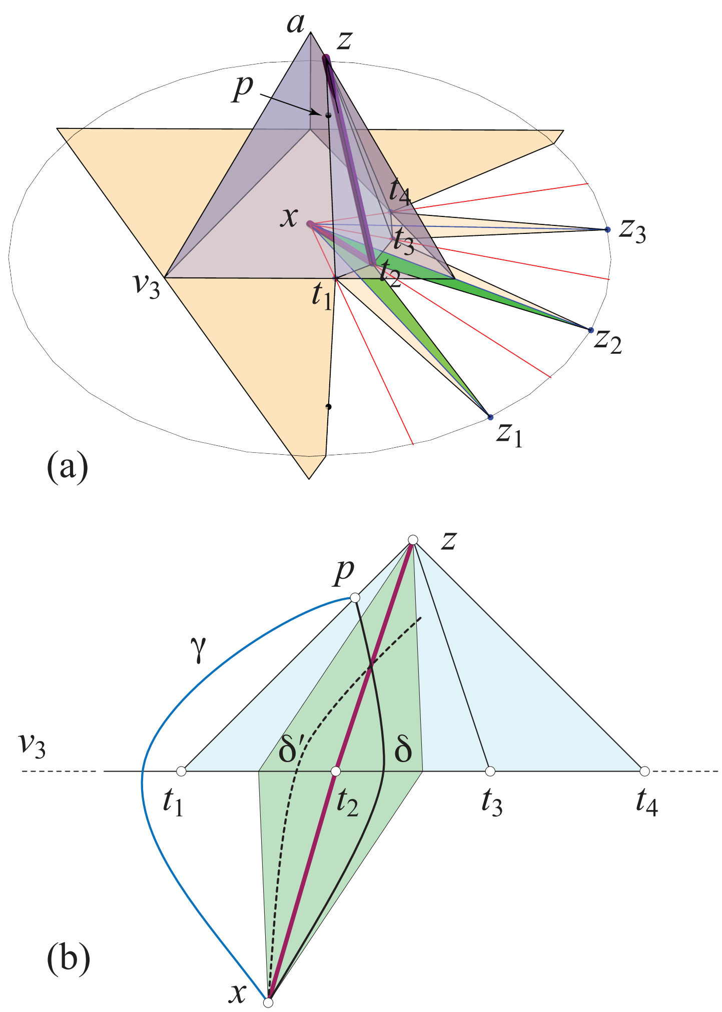

Figure 9: Proof that $p \in zt_1$ is on $\mathcal{C}(x)$. (a) Quasigeodesic $q_2 = xt_2z$ shown purple and congruent triangles xt_2z_1 and xt_2z_2 shaded green. (b) Abstract picture depicting geodesic segments γ, δ, δ'.

local intrinsic symmetry about q_3, and shows that δ cannot be a shortest path beyond q_3.

We have established that every point p on zt_1 is on $\mathcal{C}(x)$, and so $zt_1 \subset \mathcal{C}(x)$. The same argument applies to zt_{k+1}, the rightmost truncation edge in the figures.

So now we know that two geodesic segments from x to z cross t_1t_2 and t_kt_{k+1}. These two segments determine a digon D within which the remaining segments of $\mathcal{C}(x)$ lie. But within D we have local intrinsic symmetry with respect to the quasigeodesics $q_i = xt_iz$, because q_i is surrounded by the congruent triangles xt_iz_{i-1} and xt_iz_i. Therefore, the previous argument shows that all the edges zt_i are included on $\mathcal{C}(x)$. □

We now return to the claim that the three subtrees descendant from a do not interfere with one another.

Lemma 3 *The truncations for one subtree descendant of apex a do not interfere with another subtree descendant.*

Proof: First, as $k \to \infty$, t_1 approaches the line xz_0. This is evident in Fig. 12 where $k = 8$. Thus the leftmost truncation triangle stays to the v_1-side of the midpoint of v_1v_3, say by ε. Second, subsequent truncations to all but the extreme edges zt_1 and zt_{k+1} stay inside the $t_1, \ldots, t_k$ chain. The only concern would be that truncation of the zt_1 edge crossed the midpoint of v_1v_3 (and so possibly interfering with truncations of av_3). However, as is evident in the earlier Fig. 3, the position of t_1 moves monotonically toward v_1 as z moves down av_1. Thus we can widen ε to accommodate a truncation of zt_1 (or of zt_{k+1}). So the entire subtree rooted at z stays between the midpoints of v_1v_3 and v_1v_2. □

Further examples are shown in Section 10: $k = 4$ in Figs. 10 and 11, and $k = 8$ in Figs. 12 and 13.

Lemmas 2 and 3 together establish this case of Theorem 1: $\mathcal{C}(x) \subset \mathrm{Sk}(P)$ matches the given $\mathcal{T}$.

In this section we proved Theorem 1 for trees $\mathcal{T}$ without degree-2 nodes. Our construction can be viewed as realizing degree-2 nodes of $\mathcal{T}$ with flat "vertices" on $\mathrm{Sk}(P)$—points interior to edges of P. The passage from flat vertices to positive curvature vertices is a long proof,[6] accomplished in the following, after giving a few more examples for the current construction in the next section.

10 Further Examples

In this section we illustrate the previous construction with more examples.

[6] In this respect, there is some similarity to the proof of Steinitz's Theorem.

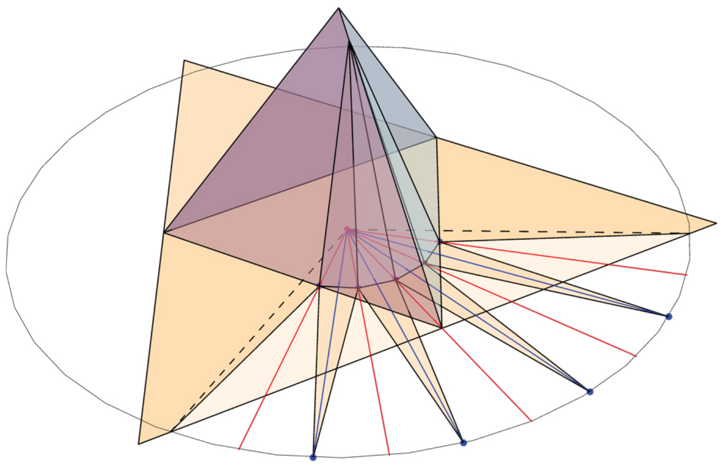

Figure 10: $k = 4$.

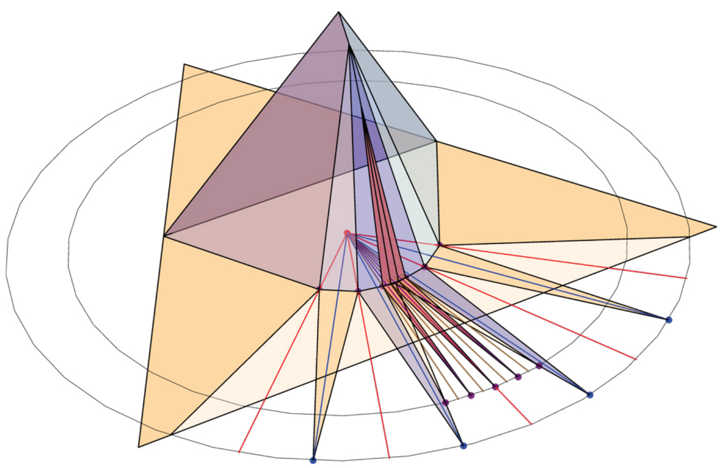

Figure 11: $k = 4$, $j = 3$.

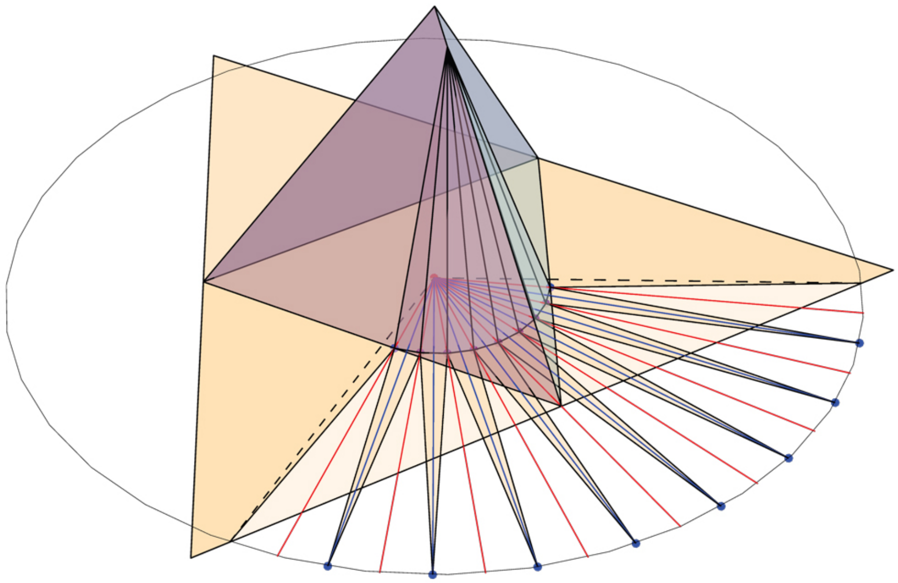

Figure 12: $k = 8$.

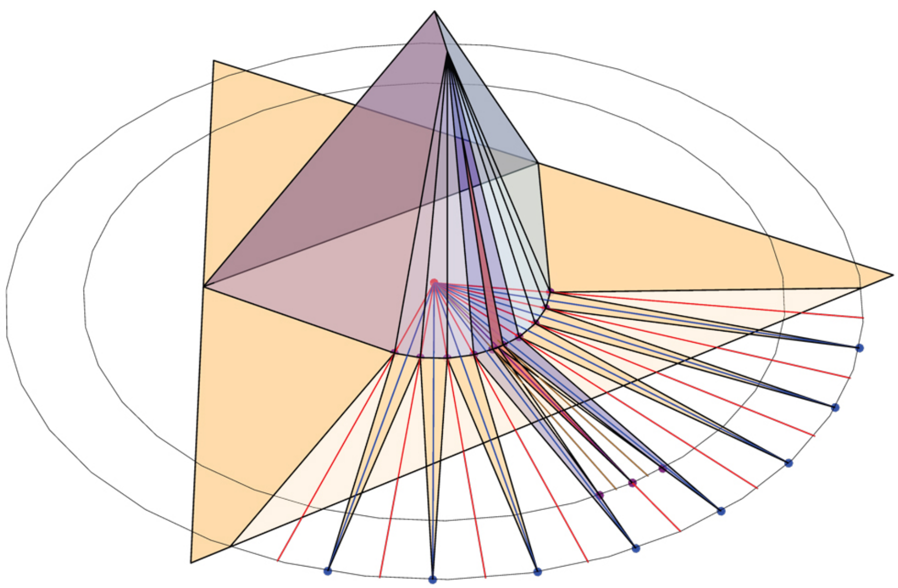

Figure 13: $k = 8$, $j = 1$.

11 Degree-2 Nodes: Four Cases

We turn now to degree-2 nodes. The overall plan is to start with a zero-curvature degree-2 node u identified on an edge ab of $\mathcal{C}(x)$. Then conveniently bend the edge at u by moving b so that u gains positive curvature, while maintaining that $\mathcal{C}(x)$ includes au and ub.

The bending at u introduces two new polyhedron edges incident to u on each side. Those two new edges could both end on the base, or one terminating on the base and the other on a non-base vertex, or both edges terminating on a non-base vertices. See Fig. 14 for examples of each case, and Fig. 15 for a polyhedron falling in Case (d). Each case will be further described in the appropriate section.

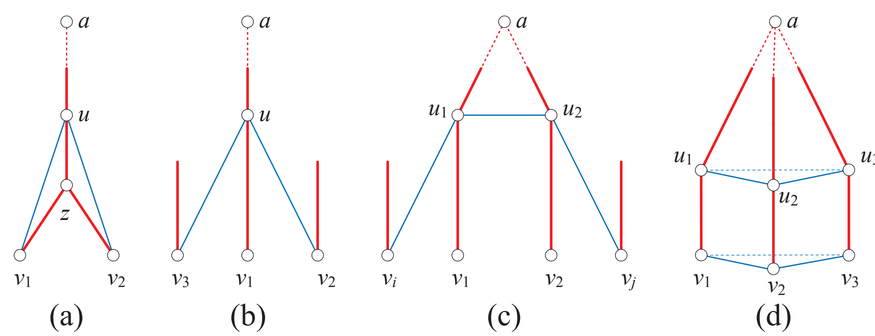

Figure 14: Examples of four cases. Red: $\mathcal{C}(x)$ edges. Blue: edges of P.

11.1 Case (a)

In both Case (a) and Case (b), a degree-2 vertex u is connected on both sides to base vertices v_i, v_j. Case (a) occurs when u is a parent of a non-base vertex z, whereas in Case (b), u is a parent of a base vertex. See Fig. 14(a,b).

In Case (a), the degree-2 vertex u can realized by modifying the construction that achieves Lemma 2. It will suffice to show how to deal with a degree-2 node u a child of apex a in the tree $\mathcal{T}$, and z a child of u of degree ≥ 3. The construction generalizes to arbitrary placements of such degree-2 nodes.

So let u be on edge av_1 but z on edge uv_1', where $v_1' \neq v_1$ is on the line segment xv_1. See Fig. 16. Thus u is a degree-4 vertex of P, but we want to arrange that two of its edges are not part of $\mathcal{C}(x)$. The two segments au and uz are in $\mathcal{C}(x)$, as they lie on the vertical symmetry plane containing axv_1.

Note that the triangle uzt_1 is not coplanar with the left face v_3t_1ua. Still, when we truncate through z, then cut the truncation edges and unfold, that triangle uzt_1 unfolds attached to the unfolding of the left face. We perform the same calculations to truncate k times at z, and the same logic (bisectors B_i and

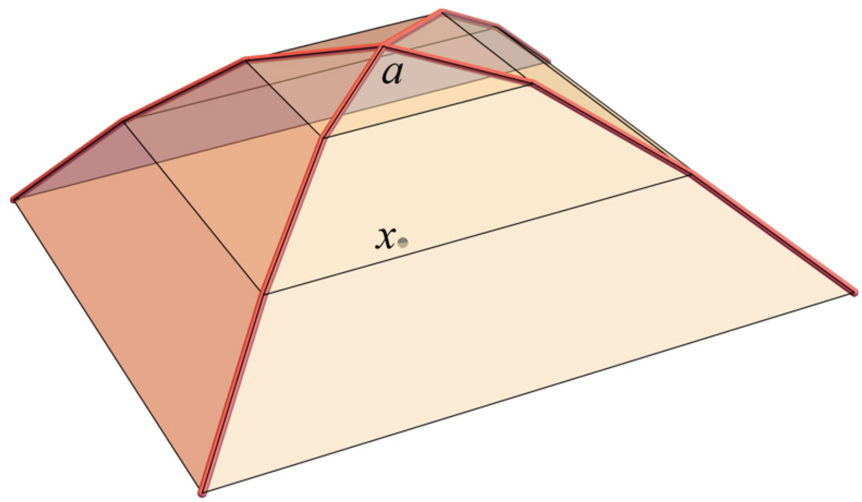

Figure 15: Case (d): Cycles of degree-2 nodes.

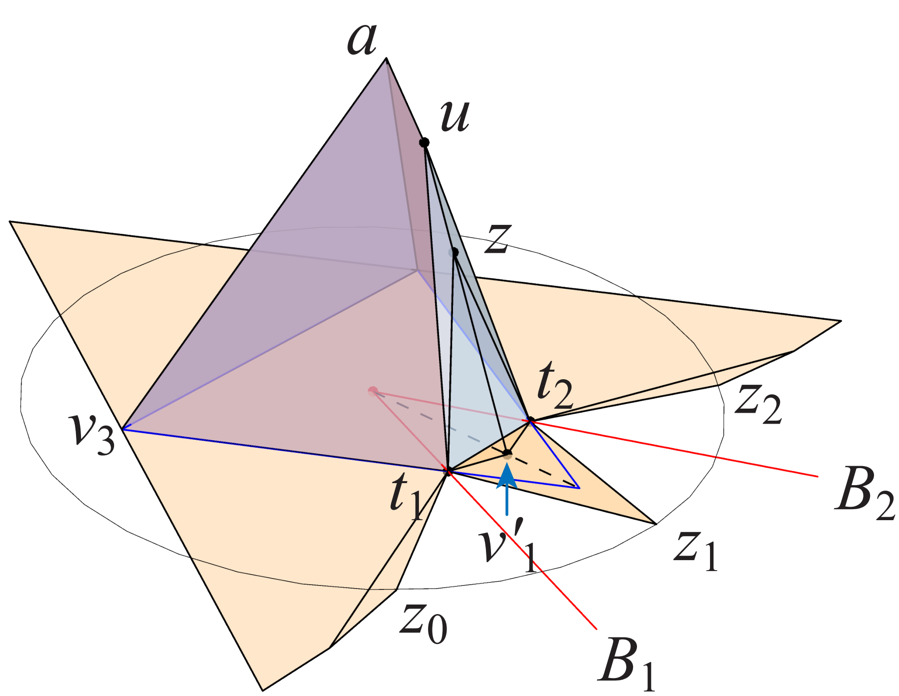

Figure 16: Case (a). u is degree-2 node. $k = 1$ truncation at z.

mediator planes Π_i) leads to the conclusion that the truncation edges are part of $\mathcal{C}(x)$.

The two side edges ut_1 and ut_2 are not part of $\mathcal{C}(x)$: a point $p \in ut_1$ is closer to x via a geodesic segment up the left face, closer than any other path from x to p. So u has degree-4 in $\mathrm{Sk}(P)$ but degree-2 in $\mathcal{C}(x)$.

11.2 Case (b)

In this case, a degree-2 node u is a parent of a leaf node v_1, as illustrated in Fig. 14(b). This requires the two non-$\mathcal{C}(x)$ edges incident to u to connect to adjacent base vertices v_2 and v_3, and consequently to other branches of $\mathcal{C}(x)$.

We confine ourselves now to starting with a regular tetrahedron with x at the centroid of the base and a the apex, as in Case (a). We first describe the construction at a high level, concentrating on v_3, with the understanding v_2 will be handled similarly.

For the regular tetrahedron, the surface angle incident to v_3 can be partitioned into two halves, to each side of the path $q = xv_3 \cup v_3a$, α to the left of q, with $\alpha = \angle xv_3v_2 + \angle v_2v_3a$, and β to the right of q, with $\beta = \angle xv_3v_1 + \angle v_3v_3a$. Because $\alpha = \beta$, the edge $v_3a \subset \mathcal{C}(x)$. Introducing u on the path auv_1 modifies the angle at v_3 to the right, to $\beta' < \beta$, breaking the bisection. So our goal is to temporarily increase β' by altering the path auv_1, so that by further truncations we could decrease it to α.

In particular, u will connect to $v_1'' \neq v_1$. (See ahead to Fig. 18.) The vertices v_2, v_3, a and the source x remain unaltered, which ensures the changes are localized, and that the construction generalizes beyond the regular tetrahedron.

Let v_1' be a point on the ray xv_1, beyond but close to v_1. (For now, this slightly increases β'.) We'll place u on the segment av_1'. But first we locate an auxiliary variable point $y \in av_1'$ which will bound u to lie above y on the segment ya. The construction will work for any u in that range.

Let y_1 be the vertical projection of y onto xv_1'. Now consider the polyhedron $P = \mathrm{conv}\{v_2, v_3, a, y, y_1\}$. We examine the angle δ incident to v_3 from the right of the path q. Angle δ will serve as β'. It is composed of three angles: on the base, the face including vertical edge $y\,y_1$, and the face including a:

$$\delta = \angle xv_3y_1 + \angle y_1v_3y + \angle yv_3a \; .$$

See Fig. 17.

Next view $y = y(t)$ as continuously varying on av_1', with $y(0) = a$ and $y(1) = v_1'$. So $\delta = \delta(t)$ is also varying continuously. We now argue that the extreme values of δ are less than and respectively greater than the fixed angle α.

- At $t = 0$, $\delta(0) = \angle xv_3a$ because the first two angle terms are zero when $y\,y_1 = ax$. This angle $\delta(0)$ is smaller than α because it is smaller than each of the two angles comprising α.

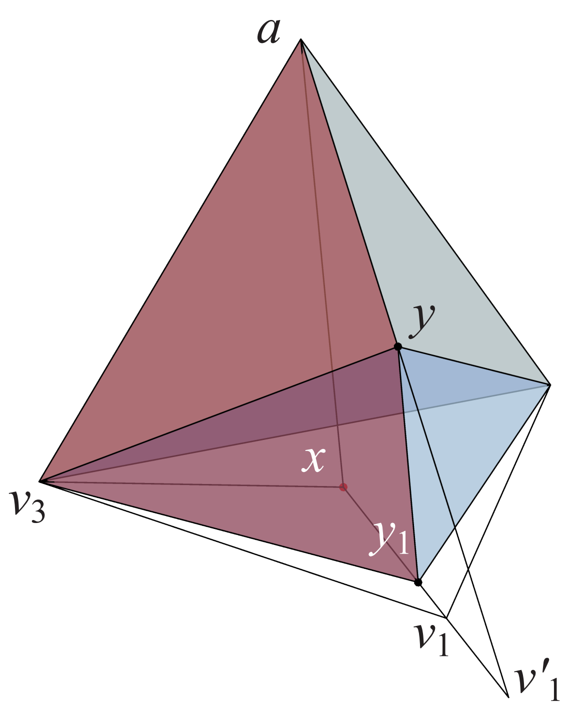

Figure 17: Case (b). The total angle at v_3 is $\angle x v_3 y_1 + \angle y_1 v_3 y + \angle y v_3 a$.

- At $t=0$, $\delta(1) = \angle x v_3 v_1' + \angle v_1' v_3 a$, because $y = y_1 = v_1'$. This angle $\delta(0)$ is larger than α by the triangle inequality for spherical distances (see e.g., Lemma 2.8 in [OV24a]).

Therefore, there is some t such that $\delta(t) = \alpha$. We henceforth define y to be that $y(t)$. The resulting polyhedron $P = P(t)$ achieves $\alpha = \beta$. Thus if we place u at y, we have achieved our goal of increasing β' to β, and thus ensuring that $v_3 a \in \mathcal{C}(x)$. However, for more complicated trees, we may need to truncate the vertical edge $y\,y_1$, so we would like choose u to slant to v_1''.

We now claim that there is some v_1'' on xv_1' such that the three angles to the right of q sum to exactly α. The analogous three angles are as in the δ argument above; see Fig. 18.

$$\angle x v_3 y_1 + \angle y_1 v_3 u + \angle u v_3 a < \alpha \ .$$

$$\angle x v_3 v_1' + \angle v_1' v_3 u + \angle u v_3 a > \alpha \ .$$

Therefore there is some $v_1'' \in y_1 v_1'$ so that the construction using the slanted edge uv_1'' achieves α, guaranteeing that $\alpha = \beta$ and $v_3 a \in \mathcal{C}(x)$. (Note that v_1'' could be closer to x than v_1, or further.)

As in Case (a), the two segments au and uv_1'' are in $\mathcal{C}(x)$, as they lie on the vertical symmetry plane containing axv_1''.

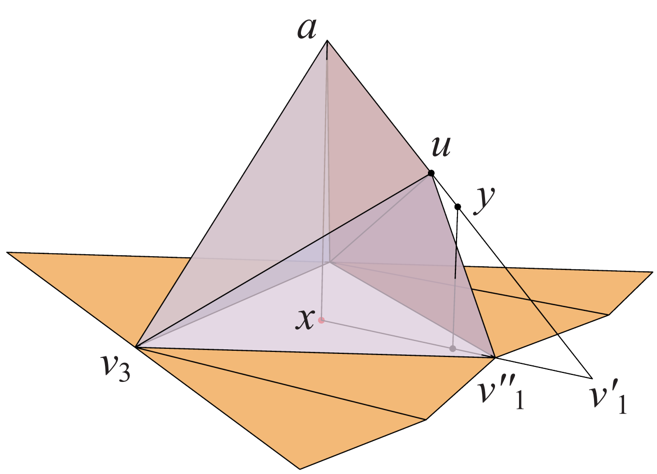

Figure 18: Case (b): Source unfolding after locating $v_1'' \in y_1 v_1'$.

We note here that, if there are several nodes of degree-2 falling under Case (b) in a cascade, they should be treated together by a similar procedure.

11.3 Case (c)

It is characteristic of Case (c) that a chain C of degree-2 nodes, represented by the single edge u_1u_2 in Fig. 14(c), connects to base vertices v_i, v_j, $1 \le i < j \le n$, on either end of C. In contrast, in Case (d) the chain closes to itself, as in Fig. 15.

The proof in Case (c) is quite involved and comprises several steps. Some of those steps describe the construction, while the others give the necessary argument for the construction to work. The proof falls roughly into two parts, the distinction of which will be useful for Remark 2 at the end of the proof. **Part I** (Item (1) to Item (11)) finds the points a_{13}, u_{13}, and then **Part II** (Item (12) to Item (23)) finds the points $a_{12}, u_{12}, y_1, u_{21}$. These points will be defined as they occur in the proof.

Part I.

(1) Start with the regular tetrahedron[7] $S = av_1v_2v_3$, and let x be the projection of a on the base plane $\Pi_b = v_1v_2v_3$.

Take $v_3' \in [xv_3]$.

This has two purposes. One is to destroy the chance of obtaining in the end as a solution precisely the original tetrahedron S. The other one is to assure the convexity of the resulting polyhedron R, and will become apparent at Item (22).

Denote by T the tetrahedron $av_1v_2v_3'$.

(2) Choose $u_1 \in [av_1]$ and take $u_2 \in [av_2]$ such that $|au_1| = |au_2|$.

Fig. 19 illustrates the setup so far. The vertices $\{v_3', a, u_1, u_2\}$ will henceforth remain fixed. The plan is to move v_1v_2 parallel to itself toward x, to y_1y_2. This will introduce a bend at u_1 and u_2. The remainder of the argument aims to calculate y_1y_2 so that $\mathcal{C}(x)$ includes au_1y_1 and au_2y_2.

It may help to look ahead to the final construction: see Fig. 24. In some sense, we are constructing the source unfolding of the "to-be-found" polyhedron.

Because of the symmetry of T, we will concentrate on the u_1 side of T.

The triangle $v_3'au_1$ of T is now fixed; it will become a face of the final polyhedron.

In the source unfolding, it will become $v_3'a_{13}u_{13}$. A key is locating this unfolded face, i.e., determining the position of a_{13}.

(3) Let θ_{13}, θ_{12} be the angles at the apex a:

$$\theta_{13} = \angle u_1av_3' \text{ and } \theta_{12} = \angle u_1au_2.$$

A key angle will be $\theta_{13} - \theta_{12}/2$. Assuming the construction is finished and looking ahead, the argument will partition θ_{13} as follows; see Fig. 20.

[7] The proof works, with minor changes, for arbitrary regular pyramids.

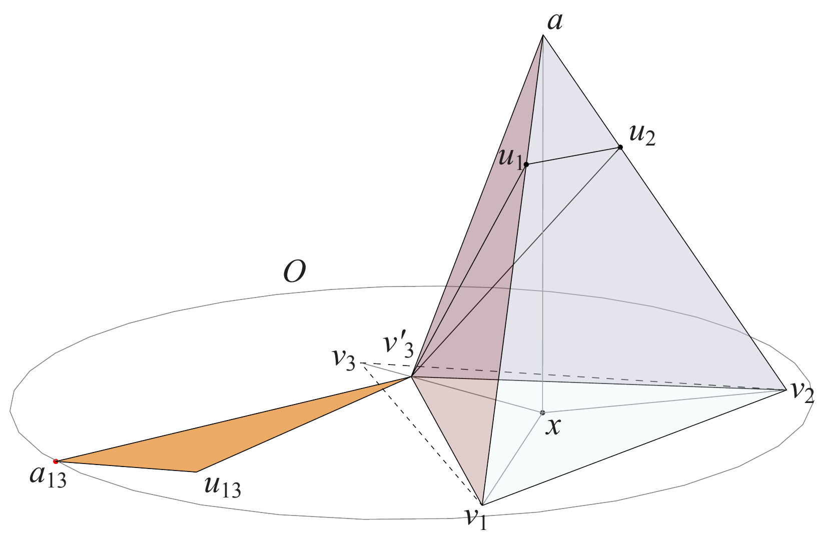

Figure 19: v_3 has been moved to v_3'. The unfolding of face $v_3' a u_1$ is shown.

$$
\begin{aligned}
\theta_{13} &= \angle u_1 a v_3' \\
&= \angle u_{13} a_{13} v_3' \\
&= \angle x a_{13} v_3' + \angle x a_{13} u_{13} \\
&= \angle x a_{13} v_3' + \angle x a_{12} u_{12} \\
&= \angle x a_{13} v_3' + \theta_{12}/2 \\
\theta_{13} - \theta_{12}/2 &= \angle x a_{13} v_3'
\end{aligned}
$$

(4) Notice that the source unfolding of the target polyhedron R would produce a point a_{13} (an image of a) in Π_b with $|a_{13} v_3'| = |a v_3'|$. So we consider in Π_b the circle O centered at v_3' and radius $|a v_3'|$, and will determine $a_{13} \in O$ by Items (5) and (7).

Notice that x is inside O.

(5) **Lemma 4** *Consider a variable point $z \in O$. The extreme values of $\phi = \phi(z) = \angle x z v_3'$ are as follows.*

The minimum value of ϕ is 0, achieved precisely for z, x, v_3' collinear.

The maximum ϕ_0 of ϕ is obtained precisely for zx perpendicular to xv_3', hence for two positions of z.

Moreover, on each of the four arcs of O determined by those extreme values, $\phi(z) = \angle x z v_3'$ is a strictly monotone function on z.

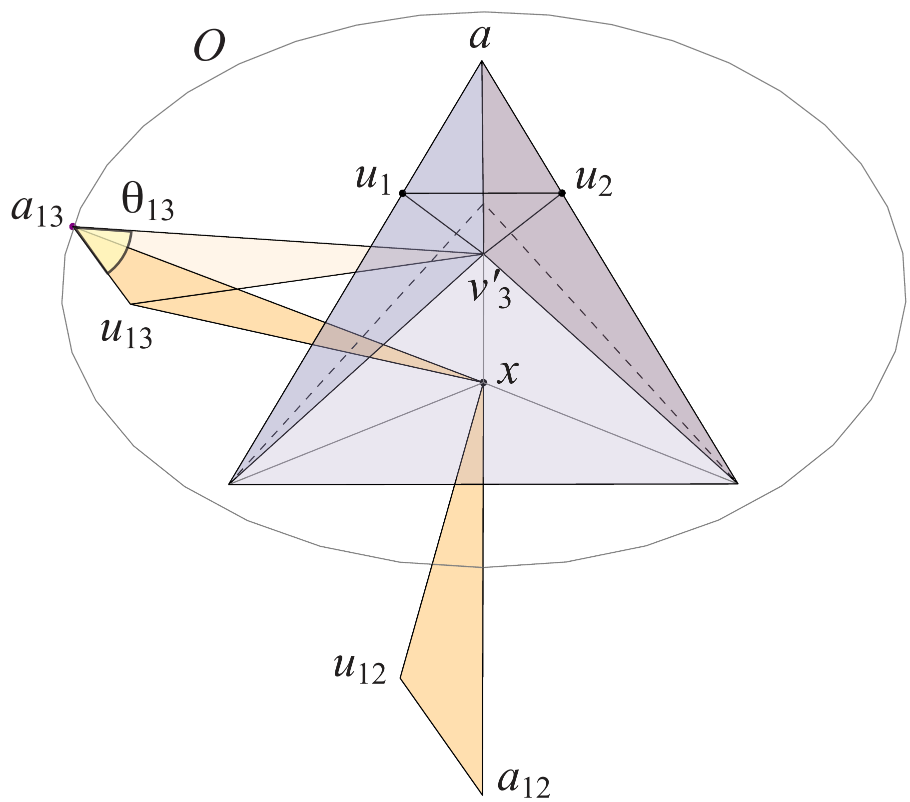

Figure 20: $\theta_{13} - \theta_{12}/2$. The labeled points a, u_1, u_2 are above the base plane, and all the other labeled points lie in the base plane.

Proof: The "minimum" claim is clear: there are precisely two positions of $z \in O$ for which the mimimum value of ϕ is attained, say at the north and the south poles of O.

To prove the rest, take the height from v_3' in the triangle $v_3'xz$, and notice that it is smaller than, or equal to, $[xv_3']$. Therefore, because sin is an increasing function, we get the two positions $z_0 \in O$ of z obtaining maximal value ϕ_0 of ϕ: $z_0x \perp xv_3'$. One of them is in the left semi-circle of O and another one in the right half-circle.

The monotonicity of the angular function $\phi(z)$ on each of the resulting four arcs is elementary. □

We will denote z_0 by a_0.

(6) Lemma 4 helps to prove the following.

Lemma 5 *There exist precisely four positions z_{13} of the variable point $z \in O$ s.t.*

$$\angle xz_{13}v_3' = \theta_{13} - \theta_{12}/2.$$

We described above in Item (3) why the angle $\theta_{13} - \theta_{12}/2$ is the appropriate choice to determine the position of a_{13} on O.

Proof: Notice that the variable ϕ defined in Lemma 4 clearly depends continuously on z, and

$$0 < \theta_{13} - \theta_{12}/2 < \phi_0, \tag{1}$$

where 0 is the minimal value of ϕ, and ϕ_0 is its maximal value given by Lemma 4.

The first inequality follows for the regular tetrahedron from the numerical values $\theta_{13} \approx \pi/3$ (for v_3' close to v_3) and $\theta_{12} = \pi/3$.[8]

To see that $\phi_0 > \theta_{13} - \theta_{12}/2$, consider $a_0 \in O$ such that $a_0x \perp xv_3'$. The triangles a_0xv_3' and axv_3' are congruent, because x is the projection of a on Π_b.

Next we show that

$$\angle xav_3 > \angle v_1av_3/2 = \angle v_1av_3 - \theta_{12}/2.$$

To see this, let $xp \perp v_3v_1$, with $p \in v_3v_1$. The theorem of the three perpendiculars implies $ap \perp v_3v_1$, hence

$$\sin(\angle v_1av_3/2) = \sin\angle pav_3 = |pv_3|/|av_3| < |xv_3|/|av_3| = \sin\angle xav_3.$$

For v_3' close enough to v_3 we have $\angle xav_3' \approx \angle xav_3$, so we still have[9]

$$\phi_0 = \angle xav_3' > \angle v_1av_3/2 = \angle v_1av_3 - \theta_{12}/2 > \theta_{13} - \theta_{12}/2.$$

[8] If, instead of the regular tetrahedron, we would start with an arbitrary regular pyramid, we would use Lm.2.8 in [OV24a] to derive the conclusion.

[9] This argument is valid for arbitrary regular pyramids.

By the continuity of ϕ and the inequalities (1), there are precisely four intermediate positions of $z \in O$ for which $\angle x z_{13} v_3' = \theta_{13} - \theta_{12}/2$. In the left semi-circle of O, one is below and one is above the point z_0 realizing the maximum of ϕ (i.e., $z_0 \in O$, $z_0 x \perp x v_3'$). $\square$

(7) Fig. 21 shows the position of z_{13} we choose for (i.e., denote by) a_{13}: the left one above z_0. This choice will be important at Item (9).

(8) Construct the triangle $v_3' a_{13} u_{13}$ congruent to $v_3' a u_1$, with u_{13} inside the angle $\angle x v_3' a_{13}$.

(9) Rotate the triangle $v_3' a v_1$ about $v_3' v_1$ until it lies in the base plane, and denote by a' the resulting image of a farthest from v_2, so a' clearly lies in the left half-circle of O.

It follows that a' is above a_{13}; i.e., a_{13} lies between a_0 and a', on the left half of O. This is a direct consequence of Items (6), (7), (10), and Lemma 6.

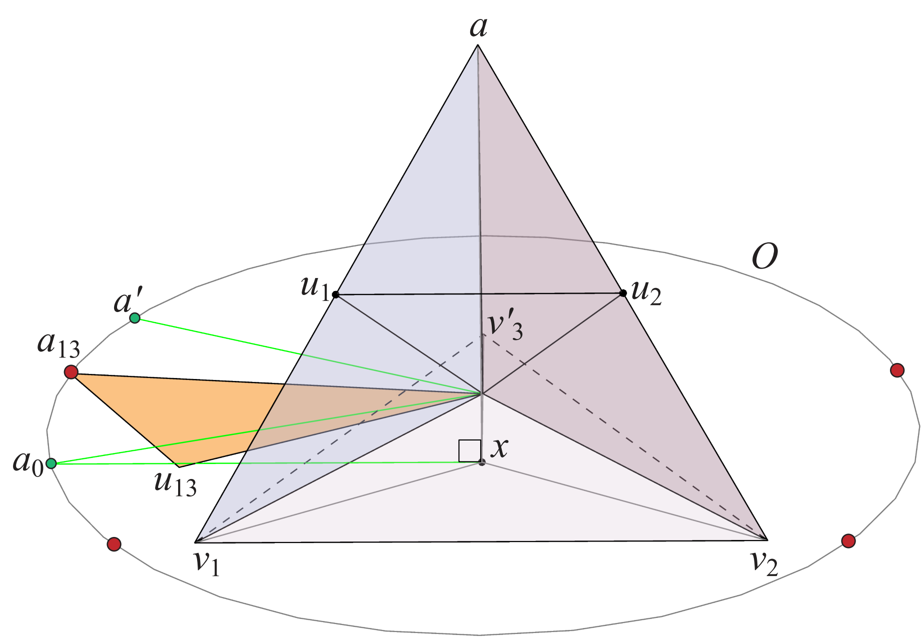

Figure 21: The four ϕ solutions (red), and a_{13} between (green) points a_0 below and a' above. The labeled points a, u_1, u_2 are above the base plane, and all the other labeled points lie in the base plane.

(10) **Lemma 6** $\angle v_3' a' x < \theta_{13} - \theta_{12}/2$.

Proof: Notice that the claimed inequality is equivalent to $\theta_{12}/2 < \theta_{13} - \angle v_3' a x = \angle x a v_1$.

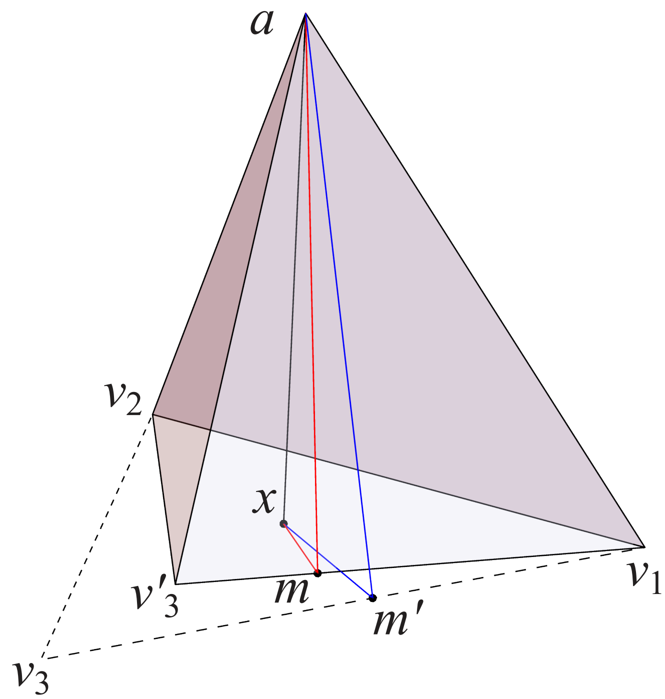

Figure 22: $xm \perp v_1v_3'$ and $xm' \perp v_1v_3$. The geoseg xma (red) on T is shorter than $xm'a$ (blue) on S.

Let $m \in v_1v_3'$ such that $xm \perp v_1v_3'$. See Fig. 22.

By the theorem of the three perpendiculars, $am \perp v_1v_3'$, so the path xma is a geodesic segment. Therefore, $\angle xav_1 > \angle mav_1$.

In the tetrahedron $S = av_1v_2v_3$, let $m' \in v_1v_3$ such that $xm' \perp v_1v_3$. Then, again by the theorem of the three perpendiculars, $am' \perp v_1v_3$, so the path $xm'a$ is a geodesic segment on S. Therefore, $\theta_{12}/2 = \angle v_3av_1/2 = \angle m'av_1$.

So the claimed inequality is reduced to $\angle mav_1 > \angle m'av_1$. This follows from $\angle mv_1a < \angle m'v_1a$, which is a direct consequence of the choice of v_3' between x and v_3. $\square$

(11) The above argument also shows that $|xm| < |xm'|$ and $|ma| < |m'a|$, hence $|xm|+|ma| < |xm'|+|m'a|$. I.e., the distance from x to a is shorter on T than on S.

Moreover, because a_{13} lies between a_0 and a', on the left half of A, $|xa_{13}| < |xa'|$. Therefore, $|xa_{13}|$ is shorter than the distance from x to a on S.

This concludes identifying the points a_{13}, u_{13}.

Part II

(12) Now we begin the second part of the proof, identifying the points $a_{12}, u_{12}, y_1, u_{21}$.

On the ray at x orthogonal to v_1v_2, take the point a_{12} determined by $|xa_{13}| = |xa_{12}|$.

(13) Construct, inside $\angle a_{12}xa_{13}$, the triangle $a_{12}xu_{12}$ congruent to $a_{13}xu_{13}$. We illustrated this step earlier in Fig. 20.

Clearly, the triangle $a_{13}xu_{13}$ lies inside $\angle v_3xv_1$, hence the triangle $a_{12}xu_{12}$ lies inside $\angle v_2xv_1$. Therefore, the triangles $a_{12}xu_{12}$ and $a_{13}xu_{13}$ share only the point x.

(14) The mediator plane Π_{13} of u_1, u_{13} intersects the plane Π_b under the line L_{13} through v_3'.

The point y_1 we are constructing should be at equal distances from u_1, u_{13}, and from u_{12}. That $|y_1u_1| = |y_1u_{13}|$ is achieved by Π_{13}, and that these distances equal $|y_1u_{12}$ is achieved by Π_{12}.

Consider $u' \in a'v_1$ such that $|a'u'| = |au_1|$. Moving continuously v_3 to v_3' would move continuously several objects: a' to a_{13}; u' to u_{13}; the mediator plane Π_1' of u_1, u' to Π_{13}; and the intersection line $v_3'v_1 = \Pi_1' \cap \Pi_b$ to L_{13}.

Therefore, because a_{13} lies between a_0 and a' (see Item (9)), L_{13} enters at v_3' the triangle $v_3'v_1v_2$ and consequently it intersects the edge v_1v_2.

(15) The mediator plane Π_{12} of u_1, u_{12} intersects the plane Π_b under the line L_{12}. Because of Item (11), L_{12} separates x from v_1v_2.

Denote by y_1 the intersection point of L_{13} and L_{12}.

Then, by Item (14), y_1 lies inside the triangle $v_1v_1v_3'$.

(16) It follows that $\angle u_1 v_3' y_1 = \angle u_{13} v_3' y_1$, hence the triangle $y_1 v_3' u_{13}$ folds to the face $y_1 v_3' u_1$.

(17) Furthermore, by Item (8), the triangle $v_3' u_{13} a_{13}$ folds to the face $v_3' u_1 a$.

(18) Proceed similarly for u_2, to obtain the points $a_{23} \in O$, u_{23}, u_{21} and y_2. The construction is symmetric with respect to the plane $axv_3' \perp v_1 v_2$.

(19) Notice that the triangles au_1u_2 and $a_{12}u_{12}u_{21}$ are congruent, as they have congruent sides from a resp. a_{12}, $au_1 \equiv a_{13}u_{13} \equiv a_{12}u_{12}$ (by Items (8) and (13)), and congruent angles between those sides (by the choice of a_{13} at Item (7) and the consecquent costruction). So $|u_1u_2| = |u_{12}u_{21}|$.

(20) Because we have $|u_{12}y_1| = |u_1y_1| = |u_{13}y_1|$ (see Items (14)-(15)) and similarly for u_{21}, and by $|u_1u_2| = |u_{12}u_{21}|$, the isosceles trapezoids $u_1u_2y_2y_1$ and $u_{12}u_{21}y_2y_1$ are congruent.

Therefore, the pentagon $a_{12}u_{12}y_1y_2u_{21}$ folds to the faces au_1u_2 and $u_1u_2y_2y_1$.

Moreover, because $u_1u_2 \parallel v_1v_2$, L_{12} is also parallel to v_1v_2.

(21) Because $|y_1u_{13}| = |y_1u_1| = |y_1u_{12}|$, we have $\angle xy_1u_{13} = \angle xy_1u_{12}$. Therefore, the edge y_1u_1 is in $\mathcal{C}(x)$, by the bisecting property of $\mathcal{C}(x)$ at y_1.

By construction, we have that $\angle a_{13}u_{13}y_1 = \angle a_{12}u_{12}y_1$, hence the edge au_1 is also in $\mathcal{C}(x)$.

(22) Finally, notice that the resulting polyhedron is convex, because y_1 and y_2 lie inside the base $v_1v_2v_3'$ (Items (15) and (18)).

(23) We next argue that the angles incident to u_1 from either side—α to the left and β to the right—are equal, proving that $\mathcal{C}(x)$ bisects at u_1. It will be easiest to work with angles in the source unfolding. So

$$\alpha = \angle y_1u_{13}a_{13}$$
$$\beta = \angle y_1u_{12}a_{12}$$

Now re-interpret these angles from x: see Fig. 23:

$$\alpha = \angle xu_{13}a_{13} + \angle xu_{13}y_1$$
$$\beta = \angle xu_{12}a_{12} + \angle xu_{12}y_1$$

By construction (Item (13))

$$\angle xu_{13}a_{13} = \angle xu_{12}a_{12}$$

and the triangles $xu_{13}y_1$ and $xu_{12}y_1$ are congruent as all their respective edges are congruent. Therefore $\alpha = \beta$.

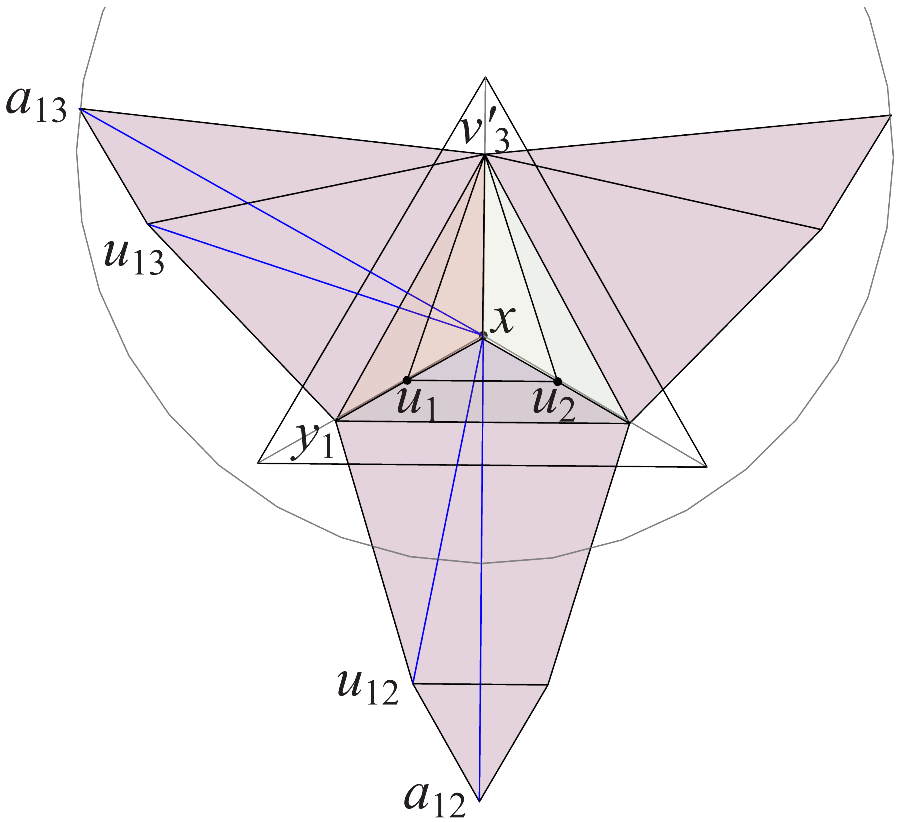

Figure 23: Overhead view. $\alpha = \beta$.

Fig. 24 shows the completed construction for $u_1 = 0.7a + 0.3v_1$. Note that $y_1 = L_{13} \cap L_{12}$ does not necessarily lie on xv_1. And note that L_{12} is parallel to v_1v_2, but L_{13} is not parallel to v_1v_3. These details may be more evident in Fig. 25, when $u_1 = 0.4a + 0.6v_1$. In a sense, this lack of "symmetry" reflects the fact that in Case (c), the polyhedron edges left and right of u_1 have different destinations: to one side terminating on the base, to the other side terminating at u_2.

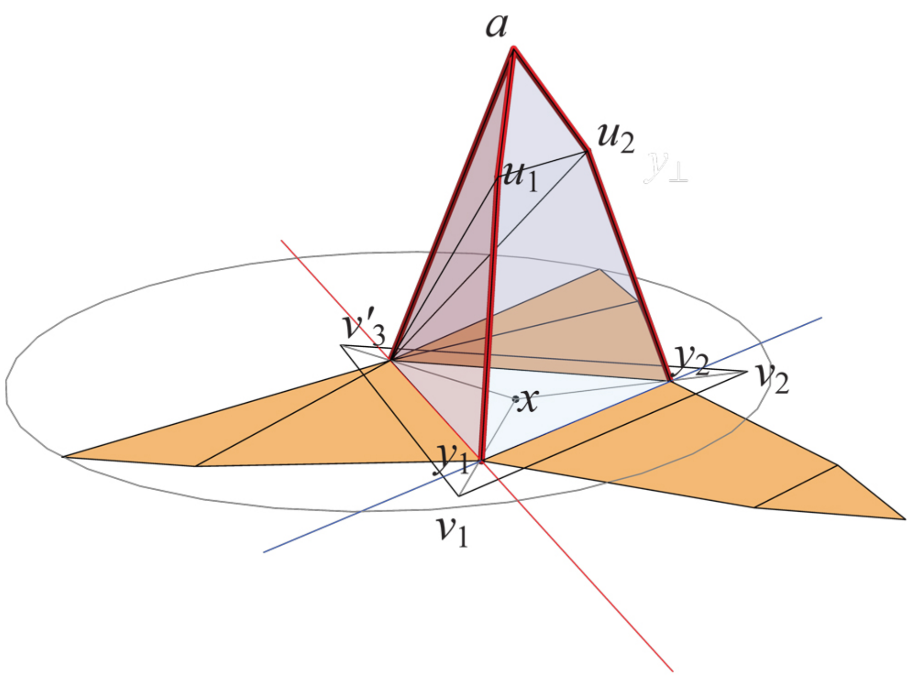

Figure 24: Final construction. u_1, u_2 at 70% of av_1

Remark 2 *Assume that, in Fig. 14(c), instead of only one blue edge u_1u_2, there is a chain C of several blue (horizontal) edges between u_1 and u_2, separated by red branches of $\mathcal{C}(x)$. Then the above construction still works: we first apply it for the two blue edges incident to u_1: a slanted one and a horizontal one; afterward we iterate only its second part, starting with Item (12).*

11.4 Case (d)

Recall that Case (d) occurs when a chain of degree-2 nodes, connected by polyhedron edges (blue in Fig. 14(d)), closes to itself, as in the polyhedron in Fig. 15.

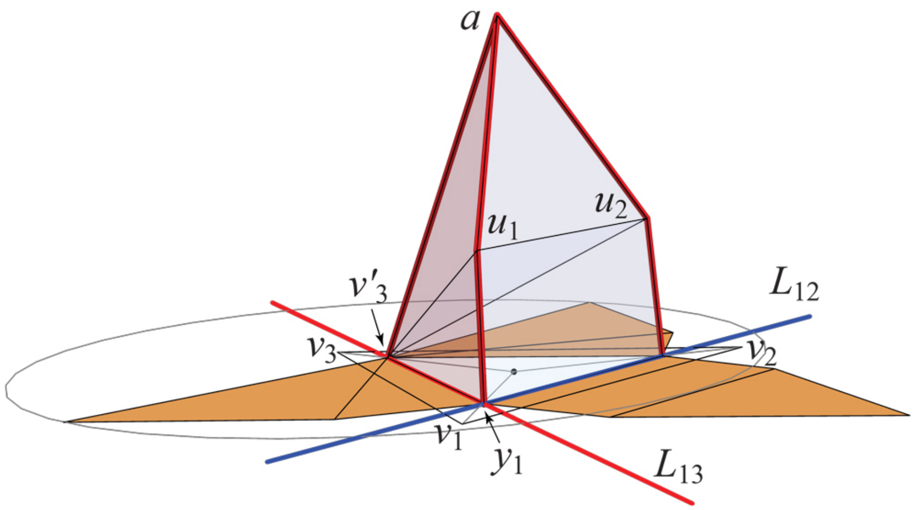

Figure 25: u_1, u_2 lower: 40% of av_1.

For simplicity of the exposition, we start with a tetrahedron $T = av_1v_2v_3$ and with the point $x \in v_1v_2v_3$ realizing a skeletal cut locus $\mathcal{C}(x)$. (The case of arbitrary pyramids is analogous.)

Our goal is to modify T by adding several nodes of degree-2 on "consecutive" branches of $\mathcal{C}(x)$, consecutive in the sense that they end at consecutive leaves v_i.

Step 1. First we show how to modify T in order to obtain a degree-2 node u_1, and later (Step 2) we explain how these modifications are compatible with modifications necessary to obtain other degree-2 nodes, on other branches of the given tree. (Step (1) shares some similarity to Case (b), Section 11.2.)

1. We focus on the edge $av_1 \subset \mathcal{C}(x)$. Denote by δ the distance on T from x to a, which is realized by three geosegs, each crossing one lateral face.

2. Consider a point y_1 on the line segment xv_1, close to v_1. Construct through y_1 the lines $L_{12} \parallel v_1v_2$ and $L_{13} \parallel v_1v_3$. See Fig. 26.

3. Consider a point u'_1 on the edge av_1. Construct through u'_1 the lines $L'_{12} \parallel v_1v_2$ and $L'_{13} \parallel v_1v_3$.

4. Truncate T with the two planes determined by $L_{12} \cup L'_{12}$, and by $L_{13} \cup L'_{13}$. Denote by P' the resulting polyhedron.

   Clearly, there are two geoarcs on P' from x to a, a "right" one and a "left" one. Because L_{12}, L_{13} are inside T, both those geoarcs are smaller than δ.

5. Now the plan is (informally) to move L'_{12} rightward until the modified right faces increase the right geoarc's distance from x to a to match δ,

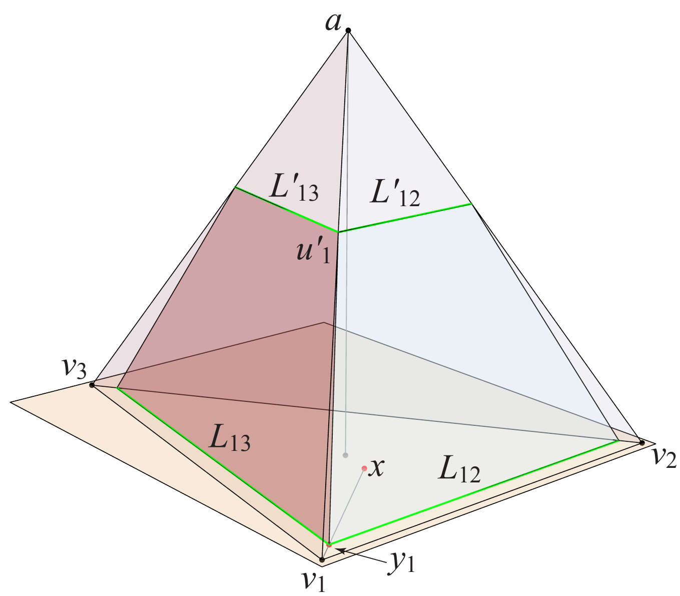

Figure 26: P': T truncated by planes through (green) lines: $L_{12} \cup L'_{12}$, and $L_{13} \cup L'_{13}$.

and then to move L'_{13} leftward to achieve the same distance δ for the left geoarc.

6. Consider a variable line Δ_z displacing continuously by a horizontal offset z from its initial position L'_{12} toward the exterior of P', maintaining at all times $\Delta_z \parallel L_{12}$.

   Denote by δ_z the length of the shortest path from x to a which crosses L_{12} and Δ_z. Clearly, δ_z increases continuously from some value $< \delta$ to arbitrarily large values. Therefore, there exists a position of D_z for which $\delta_z = \delta$. Denote by Δ_{12} this position. See Fig. 27.

7. Move continuously a variable point u along Δ_{12}, and consider the line $\Delta_u \parallel L_{13}$ through u.

   The starting position of u is when Δ_u is the supporting line of P' closer to L_{13}. The point u displaces toward the exterior of P', maintaining at all times $\Delta_z \parallel L_{13}$.

   Denote by δ_u the length of the shortest path from x to a which crosses L_{13} and Δ_u. Clearly, δ_u increases continuously from some value $< \delta$ to arbitrarily large values. Therefore, there exists a position of D_u for which $\delta_u = \delta$. Denote by Δ_{13} this position. Note that the right faces of P' are unaltered by the movement of Δ_u, so $\delta_z = \delta$ still holds. See Fig. 28.

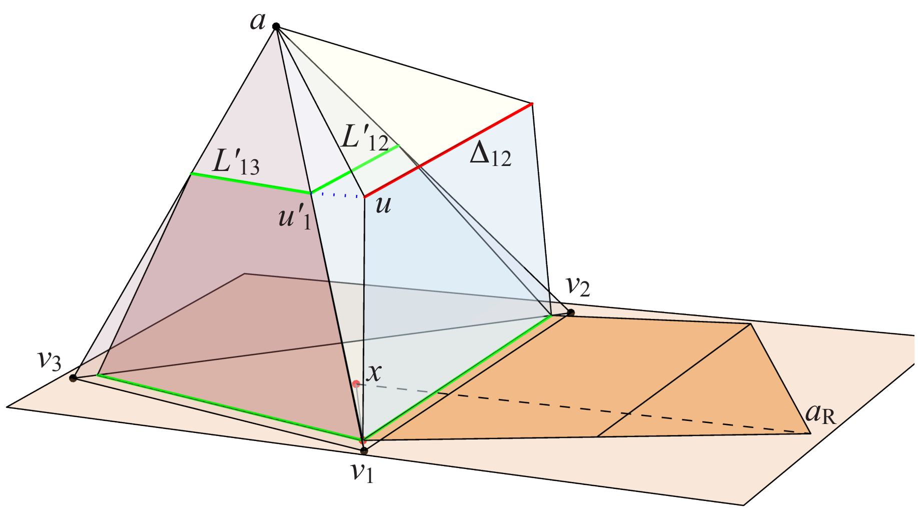

Figure 27: L'_{12} (green) $\rightarrow \Delta_{12}$ (red), when $\delta_z = \delta$. The geoseg from x to a across Δ_{12} unfolds to straight segment xa_R in the base plane.

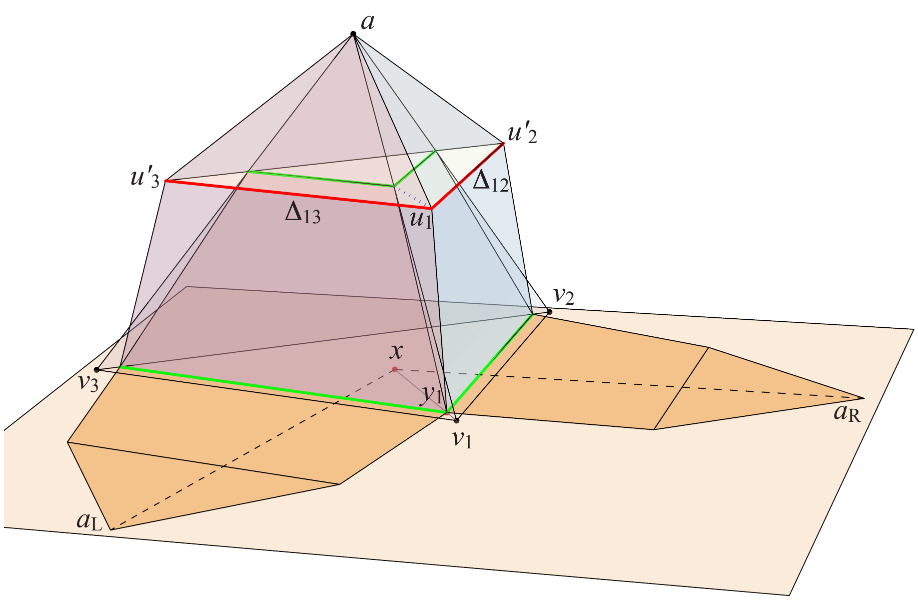

Figure 28: $u_1 = \Delta_{12} \cap \Delta_{13}$.

8. Let u_1 denote the intersection point of Δ_{12} and Δ_{13}. Let B be the plane containing the back face av_2v_3 of T.

   Put $\{u_2'\} = \Delta_{12} \cap B$, $\{u_3'\} = \Delta_{13} \cap B$, $\{y_2'\} = L_{12} \cap B$, $\{y_3'\} = \Delta_{13} \cap B$. See Fig. 29. Denote by P the convex polyhedron with vertices $a, u_1, u_2', u_3', y_1, y_2', y_3'$.

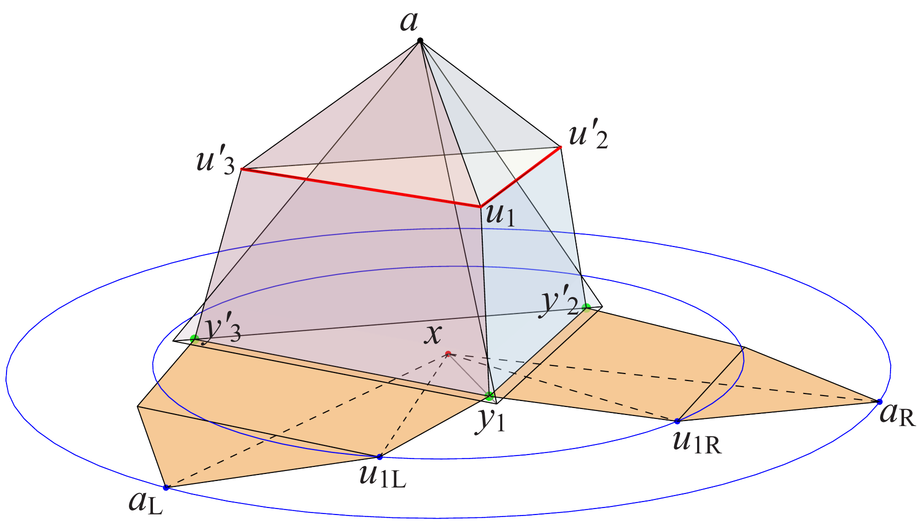

Figure 29: $P = \text{conv}(a, u_1, u_2', u_3', y_1, y_2', y_3')$. Unfolded images of xa and xu_1 shown dashed.

   Notice that P converges to T if y_1 converges to v_1.

   Let $\text{dist}^Q(x, p)$ be the distance from x to point p on polyhedron Q. To this stage of the argument, we have established that the point u_1 is exterior to T such that, on P:

   - $\text{dist}^P(x, a)$ is equal to the distance δ on T from x to a—$\text{dist}^T(x, a)$—and
   - $\text{dist}^P(x, a)$ is obtained by three geosegs: one crossing Δ_{12}, one crossing Δ_{13}, and one up the back face B, which derives from T and has remained unaltered by all previous changes.

   We thus have shown that $a \in \mathcal{C}(x)$.

9. Unfolding T and P in the base plane gives the same images a_L, a_R of a, by the choice of u_1. See Fig. 29. We next turn to showing that u_1y_1 is in $\mathcal{C}(x)$, by considering the source-unfolding images u_{1R}, u_{1L}.

10. The planar triangles xv_1a_R and xv_1a_L are congruent (all sides equal), hence $\angle y_1xa_R = \angle y_1xa_L$.

11. Therefore the triangles y_1xa_R and y_1xa_L are congruent, hence $|y_1a_R| = |y_1a_L|$ and $\angle xy_1a_R = \angle xy_1a_L$.

12. Therefore, the triangles $y_1 u_R a_R$ and $y_1 u_L a_L$ are congruent (all sides equal). So $\angle a_R y_1 u_R = \angle a_L y_1 u_L$.

13. From 11 and 12 we have $\angle x y_1 u_R = \angle x y_1 u_L$. Therefore, $y_1 u_1$ is contained in $\mathcal{C}(x)$ on P.

14. Therefore, on P, $|xu_R| = |xu_L|$. Because $a \in \mathcal{C}(x)$ on P, $au_1 \subset \mathcal{C}(x)$ on P.

This completes Step 1: both au_1 and $u_1 y_1$ are in $\mathcal{C}(x)$, and u_1 is of degree-2 in $\mathcal{C}(x)$.

Step 2. We now discuss the compatibility of the above changes around v_1/y_1 with other changes.

We take $\{y_2\} = L_{12} \cap xv_2$, and we iterate the above construction from Item 7 onward. So we identify the point $u_2 \in \Delta_{12}$ and the line Δ_{23}.

Finally, we take $\{y_3\} = L_{23} \cap xv_3$, and we iterate the above construction from Item 7 onward. This identifies the point $u_3 \in \Delta_{23}$.

It remains to prove that, by the above mentioned iterations, we close the chain of base edges joining y_i and horizontal edges joining u_i (as in Fig. 15).

First we show that the chain of base edges joining y_i closes. This follows directly from the next two pairs of similar triangles, with the same similarity ratio: xv_1v_2 and xy_1y_2, xv_2v_3 and xy_2y_3. Consequently, the triangles xv_1v_3 and xy_1y_3 are also similar with the above similarity ratio.

Now we see that the chain of horizontal edges joining u_i closes. This follows from the fact that the lengths of the geosegs on the resulting polyhedron, from x to a and crossing the respective edges, are all equal to δ.

The proof for Case (d) is thus complete.

Call the polyhedra obtained by successively applying a finite sequence of our constructions *tapered polyhedra*.

12 Induction Proof

With the four degree-2 cases settled, we can prove our main theorem.

Theorem 1 *Given any combinatorial tree $\mathcal{T}$ there is a convex polyhedron P and a point $x \in P$ such that the cut locus $\mathcal{C}(x)$ is entirely contained in* $\mathrm{Sk}(P)$, *and the combinatorics of $\mathcal{C}(x)$ match $\mathcal{T}$.*

Proof: If all nodes of $\mathcal{T}$ have degree-2 then it can be realized on a doubly covered polygon, see e.g. [OV24a, Lem.2.2].

So we may assume that $\mathcal{T}$ has at least one node of degree ≥ 3, say a. Fix the root of $\mathcal{T}$ at a; this will become the apex of the realizing polyhedron.

The proof is constructive, by induction over the discrete distance (i.e., the number of edges) to a in $\mathcal{T}$. Precisely, denote by $\mathcal{T}_k$ the subtree of $\mathcal{T}$ consisting of all nodes at distance at most k from a, together with all edges joining them in $\mathcal{T}$. We show by induction that all $\mathcal{T}_k$ can be realized as cut loci.

For $k = 1$, $\mathcal{T}_1$ has one internal node a and as many leaves as the degree of a in $\mathcal{T}$. Assume, for the simplicity of the exposition, that $\deg a = 3$. (The case $k > 3$ can be treated analogously. See Fig. 31 for an abstract example).

We realize $\mathcal{T}_1$ on a regular tetrahedron P_1, with a the top apex and x the center of the base $v_1v_2v_3$.

Assume now that we have realized $\mathcal{T}_k$ as a cut locus on a tapered polyhedron P_k with a the top apex and x the center of the base $v_1v_2v_m$, where m is number of leaves of T_k. By the induction hypothesis, P_k is obtained from P_1 by successive modifications detailed by our case constructions.

We must manage the interactions between the newly added edges to create degree-2 and degree 3 nodes. Therefore, we start with the creation of degree-2 nodes. We illustrate some cases in Fig. 30.

(1) If all branches have nodes of level k, and at least one of them is of degree-2, then we start by applying Case (d). (This occurs with nodes $2, 3, 4$ in Fig. 30(a), when Case (d) is applied). This will create the necessary degree-2 nodes; moreover, all nodes to become of degree ≥ 3 are now degree-2 nodes. After that we apply other necessary changes, to transform some of the nodes of degree 2 into nodes of higher degree, by appropriate truncations described in Section 9.

(2) Otherwise, if at least one branch has no node of level k and there are nodes of degree-2, we apply Cases (a)-(c) whichever ones are appropriate (This occurs with nodes $5, 6$ in Fig. 30(a), when Case (a) is applied). And finally,

(3) If all branches have nodes of level k and degree ≥ 3 we apply the respective construction.

This completes the induction proof and establishes Theorem 1. $\square$

We also illustrate the induction steps in a second example, shown in Fig. 31. The steps in this example are as follows:

(a) The introduction of nodes 2 and 3 creates an instance of Case (c), because node 2 is degree-2.

(b) Node 4 creates an instance of the construction in Section 9.

(c) Node 5 creates an instance of Case (b).

(d) Nodes 6 and 7 constitute an instance of Case (c).

As our goal has been proving Theorem 1, we have focussed on the existence of a realizing polyhedron P for any given tree $\mathcal{T}$. We have not addressed the algorithmic question of actually constructing P from $\mathcal{T}$. However, because all

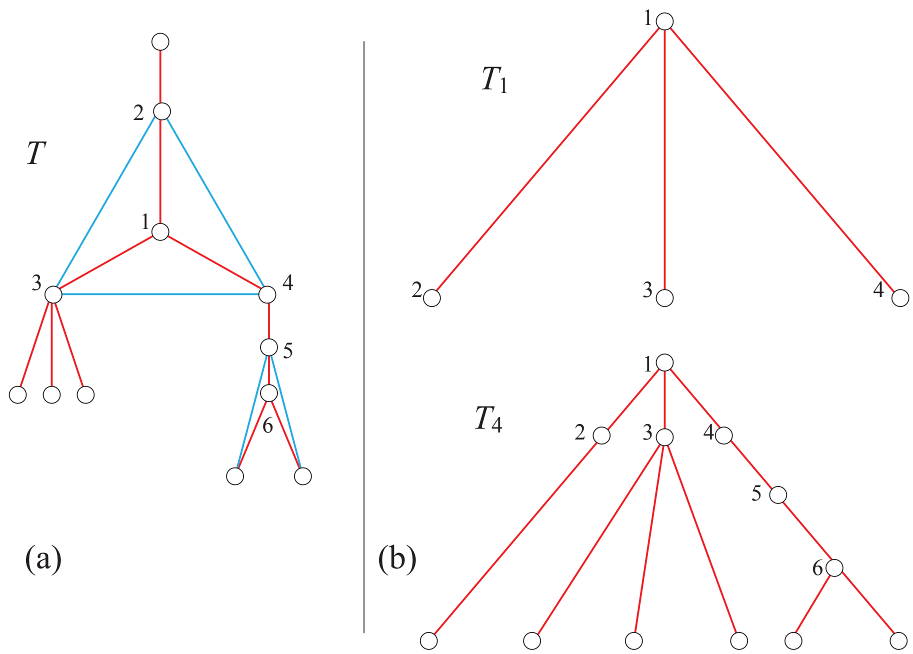

Figure 30: (a) Tree $\mathcal{T}$. Blue edges are non-$\mathcal{C}(x)$ polyhedron edges. Case (d) is applied to nodes $1, 2, 3, 4$. Case (a) is applied to nodes $5, 6$. (b) The first and last induction steps.

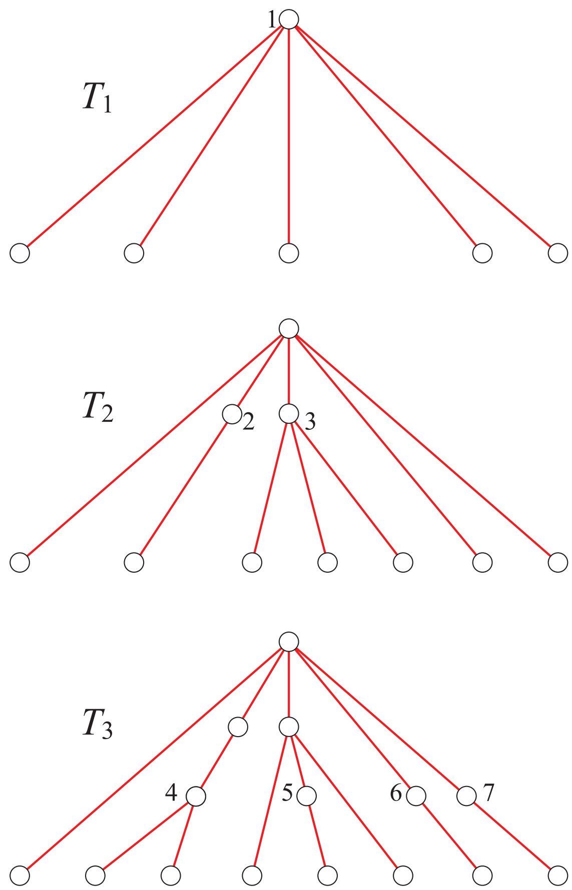

Figure 31: Example of induction construction. Two nodes $2, 3$ are added in the transition from $\mathcal{T}_1$ to $\mathcal{T}_2$, degree-2 and degree-4 respectively. Four nodes are added in the transition from $\mathcal{T}_2$ to $\mathcal{T}_3$: 4 of degree-3 and $5, 6, 7$ of degree-2.

of our constructions are explicit (and have been individually implemented), the proof in some sense already constitutes an algorithm. Without analyzing it carefully, we expect that the complexity of the algorithm is proportional to the number of nodes in $\mathcal{T}$, with some data-structure overhead. We leave establishing this formally to future work.

13 The Class of Tapered Polyhedra

As we noted in the Introduction, a polyhedron with a skeletal cut locus leads directly to an edge-unfolding to a net (a nonoverlapping polygon in the plane). This is because the source unfolding from x, which is known to be a net, is achieved by cutting the cut locus $\mathcal{C}(x)$, which maps to the outer boundary of the unfolding. Despite considerable effort by researchers to resolve Dürer's problem [O'R13]—whether or not every convex polyhedron has an edge-unfolding to a net—there are only a few infinite classes of polyhedra known to edge-unfold to a net. One class is the *domes*, polyhedra with a distinguished base face B such that every other face shares an edge with B [DO07, Sec. 25.5.2]. A slight extension to *g-domes* (generalized domes) allows a face to share just a vertex with B [OV24a, Sec. 3.1].

The main theorem of this paper leads to what we call *tapered polyhedra*, a class that properly includes some g-domes (and therefore domes). It is therefore of interest to list a few geometric characteristics of tapered polyhedra:

- Every non-base vertex projects orthogonally to be strictly inside the base.[10]
- Case (a) in Fig. 14 already goes beyond domes, to g-domes: Two triangle faces share just a vertex with the base.
- A tempered polyhedron is partitioned into zero or more "level rings" of nodes deriving from Case (d), connected in a cycle of vertices, as (for example) in Fig. 15. These rings take us beyond domes and g-domes, and so the tapered polyhedra constitute a new class of polyhedra with edge-unfoldings to nets.

We do not yet know a complete geometric characterization of tapered polyhedra.

We mention here that the order of assembling the cases to prove (by induction) Theorem 1 may differ. What we proposed in Section 12 is just one viable way, among perhaps several others. And the order of assembling the cases may result in different subclasses of polyhedra, within the class of tapered polyhedra.

We conclude by repeating this central open problem from Section 1.

Open Problem 4 *Characterize all the polyhedra P that support a skeletal cut locus, i.e., characterize the cut locus amenable polyhedra.*

[10]Basically, this was our choice to simplify the reasoning; see for example Section 9 and Fig. 3. Avoiding this choice would lead to technical difficulties we have not addressed.

References

[AAOS97] Pankaj K. Agarwal, Boris Aronov, Joseph O'Rourke, and Catherine A. Schevon. Star unfolding of a polytope with applications. *SIAM J. Comput.*, 26:1689–1713, 1997.

[DDH+11] Erik D. Demaine, Martin L. Demaine, Vi Hart, John Iacono, Stefan Langerman, and Joseph O'Rourke. Continuous blooming of convex polyhedra. *Graphs and Combinatorics*, 27:363–376, 2011.

[DO07] Erik D. Demaine and Joseph O'Rourke. *Geometric Folding Algorithms: Linkages, Origami, Polyhedra.* Cambridge University Press, 2007.

[GNRZ24] Jan Goedgebeur, Kenta Noguchi, Jarne Renders, and Carol T. Zamfirescu. HIST-critical graphs and Malkevitch's conjecture. arXiv:2401.04554., 2024.

[LP22] Nina Lebedeva and Anton Petrunin. Alexandrov's embedding theorem. arXiv:2212.10479, 2022.

[Mou85] David M. Mount. On finding shortest paths on convex polyhedra. Technical Report 1495, Dept. Computer Science, Univ. Maryland, 1985.

[O'R13] Joseph O'Rourke. Dürer's problem. In Marjorie Senechal, editor, *Shaping Space: Exploring Polyhedra in Nature, Art, and the Geometrical Imagination*, pages 77–86. Springer, 2013.

[OV23] Joseph O'Rourke and Costin Vîlcu. Cut locus realizations on convex polyhedra. *Comput. Geom.: Theory & Appl.*, 114, 2023.

[OV24a] Joseph O'Rourke and Costin Vîlcu. *Reshaping Convex Polyhedra.* Springer, 2024.

[OV24b] Joseph O'Rourke and Costin Vîlcu. Skeletal cut loci on convex polyhedra. In *36th Canad. Conf. Comput. Geom.*, pages 25–31, July 2024.

[SS86] Micha Sharir and Amir Schorr. On shortest paths in polyhedral spaces. *SIAM J. Comput.*, 15:193–215, 1986.